RAPID POST-EARTHQUAKE

STRUCTURAL ASSESSMENT USING EITHER

PEAK FLOOR ACCELERATION OR DISPLACEMENT MONITORING

by

Wael Aloqaily

A thesis submitted to the Faculty of the University of Delaware in partial fulfillment of the requirements for the degree of Master of Civil Engineering

Summer 2019

RAPID POST-EARTHQUAKE
STRUCTURAL ASSESSMENT USING EITHER
PEAK FLOOR ACCELERATION OR DISPLACEMENT MONITORING

by

Wael Aloqaily

Approved: ____
Michael J. Chajes, Ph.D.
Professor in charge of thesis on behalf of the Advisory Committee

Approved: ____
Sue McNeil, Ph.D.
Chair of the Department of Civil and Environmental Engineering

Approved: ____
Levi T. Thompson, Ph.D.
Dean of the College of Engineering

Approved: ____
Douglas J. Doren, Ph.D.
Interim Vice Provost for Graduate and Professional Education

ACKNOWLEDGMENTS

I would like to thank Fulbright, Amideast and University of Delaware for funding this research and for the consistent support their staff provided.

My Sincere thanks to my thesis advisor Prof. Michael J. Chajes who always provided guidance, knowledge, patience, time and effort and for being a source of motivation and support throughout this research. He was my coach for navigating the world of research. I owe him a lot! I would also thank all the faculty members, especially Prof. Monique Head, who all gave me the knowledge and support.

I am very grateful to my mother, father, and other family members. Their support was vital for me to overcome the hard times and keep me motivated towards completing this research.

Special thanks to university staff, particularly to Christine Reoli for her exceptional kindness and helpfulness. Without you Chris many things would have been very different!

Finally, not to forget to mention my friends and colleagues who appreciated my work and kept me proud of it all the time.

Thank you all for your support!

Wael Aloqaily

TABLE OF CONTENTS

Appendix

LIST OF TABLES

LIST OF FIGURES

ABSTRACT

In this study two approaches for rapid post-earthquake structural assessment were investigated. First, peak floor accelerations were used as an indicator for damage. Linear time-history analyses were performed using several significant earthquake records. Numerical models of undamaged four, six and eight story concrete moment resisting frames were subjected to the various earthquake records, as well as analyzing two damage states: twenty five percent damaged, and fifty percent damaged. Damage was idealized as reduction in moment of inertia of the vertical elements. The results were then compared against a number of hypotheses regarding the peak floor acceleration (PFA) profile, variance and change in peak floor acceleration due to increased damage. The PFA profile was found to be more sensitive to the ground-motion characteristics than the structural damage. The same can be said about the change in PFA with damage. The variance relationship with damage still needs more investigation. The work also includes a literature review of available damage assessment techniques using measured displacements. Finally, the applicability and limitations of each method was evaluated with digital image correlation being found to have the greatest potential to provide a low-cost structural health monitoring system for typical structures.

Chapter 1

PROBLEM

1.1 Introduction

Earthquakes are one of the most powerful natural events that exist. A simple way to define an earthquake is the shaking of earth-crust’s ground rocks; breaking to release the strain energy developed through tectonic plates movements over time. These strains are released in the form of kinetic energy; causing strong ground motions which can result in the destruction of communities, and in some cases can be strong enough to permanently deform natural features such as rivers and islands. Seismologists have been able to identify the zones where majority of earthquakes occur. They are mostly located around the edges of tectonic plates in what is known as the “ring of fire” as shown in Figure 1.1.

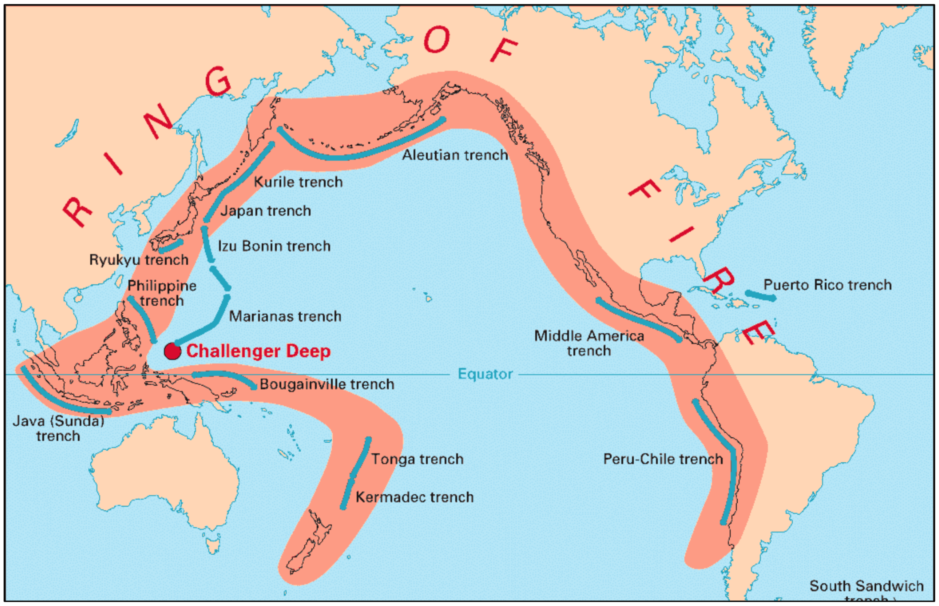

Figure 1.1 Ring of fire map from (USGS, Latest Eqarthquakes, 2019)

It can be clearly observed when taking a quick look at locations of earthquake events that happened during last year (2018) in Figure 1.2 that most of them are corresponding with the plates' boundaries shown. While the locations where earthquakes are likely to occur is well known, the timing of when earthquakes will occur is nearly impossible to predicted.

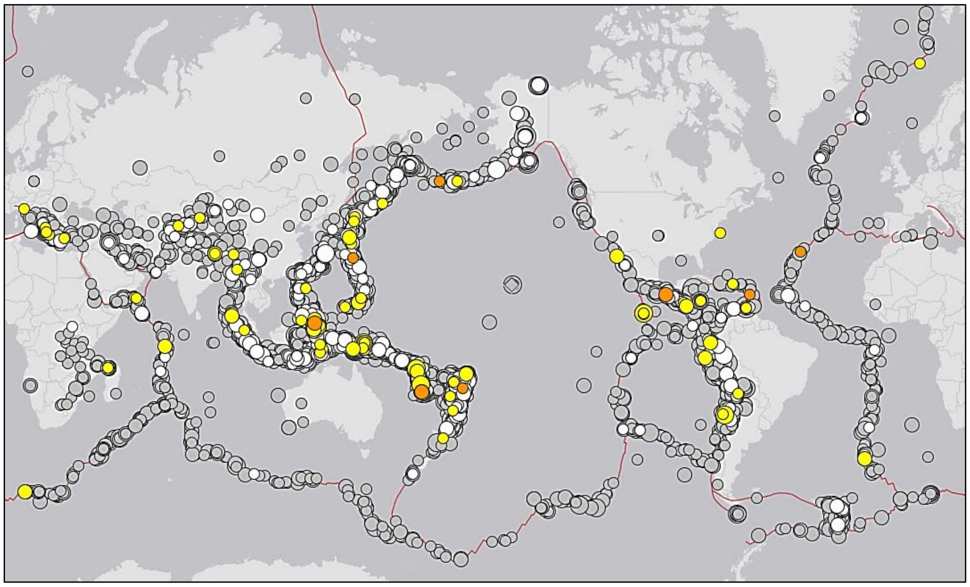

Figure 1.2 Earthquakes with (M> 4.5+) form Jan 2018 until Jan 2019 taken from USGS website (USGS, Latest Eqarthquakes, 2019)

1.2 How Do Earthquakes Affect Structures?

When the ground shakes, it displaces; creating differential movement between the base and the top of the structure, or in particular, between the substructure and the superstructure. Subsequently, such displacement is transferred along the floor levels. Depending on the stiffness of the lateral force resisting system, the displacement is then translated into stresses in vertical elements. The design philosophy for earthquake-resistant structures is built on deformation control rather than strength, in other words, damage is expected to occur, but collapse should be prevented. So, whether or not the structure was designed for earthquakes, it may experience damage which requires post-earthquake inspection and evaluation of the safety and usability of the structure.

1.3 Losses During an Earthquake Event

The inability to predict earthquakes prevents communities from preparing for specific seismic events. As a result, people suffer from different types of losses. Starting immediately during the event there can be human life losses and property damage. It’s even said that the earthquake itself doesn’t kill humans, their assets do! The effect of earthquakes extends beyond this to disruption of services and financial activities. This can take place due to the damage induced on facilities or workers to discontinuities in supply chains or the transportation lines of goods and services. In addition, infrastructure damage slows down post-event recovery. For example, damage to road networks increases the delay in evacuating injured people or time needed for firefighters to get to the scene; leading to even greater losses.

Adding on top of this are delays resulting from inspecting structures before they are put back into use. This exacerbates the challenge of restoring the built infrastructure to its pre-earthquake condition. It also includes providing temporary shelters and services for people during the inspection time. An example is the Canterbury earthquake sequence in New Zealand 2010-2011 where the direct losses were estimated to be $15.8 billion (US). In addition, the growth in economy was reduced by 1.5% in 2011 compared to the prior year, which was also reflected in tax revenues (Marshall, et al., 2013).

Utilizing modern technology and structural instrumentation (acceleration, velocity, displacement, …etc.), the time needed for inspection can be reduced. While the cost of installing and maintaining sensors is expensive, the benefits may well be worth the cost. For example, CSMIP instrumentation cost was up to $3,300 per sensor channel as estimated by Huang et al. (2002) (Huang & Shakal, 2001). Because new devices are being developed every day, the abilities of scientists and engineers to solve problems more easily expands as well, and building inspection is one of the problems that sensors can help with.

The main goal of this study is to investigate how developing structural health monitoring technologies can be used to simplify and expedite the building inspection process after earthquake; so that buildings can be put into use faster and more safely.

1.4 Challenges

Throughout this study, several challenges were faced starting from modeling, structure selection and stiffness assumption, damage simulation, modeling approach, and analysis procedure selection. Then, model reduction and earthquake record selection for the time-history analysis. Finally, in analyzing the results where multiple potential relations between peak floor accelerations and induced damage were investigated.

1.5 Structural Health Monitoring Systems

Combining sensors, networks, data loggers and other components to form a Structural Health Monitoring System (SHMS) is not a novel idea. But, as new sensors are developed and offered in the market for lower prices, the range in which SHMS can be used continues to expand. Although their name implies that such systems are designed to protect structures, that also includes human lives and other assets. The data collected by SHMSs have the potential to give engineers the ability to detect responses before they propagate to failures and translate into losses. They also provide a better understanding of the actual behavior of the structures, away from the ideal world of assumptions and computer models.

SHMSs can send data to data acquisition system, from which an engineer has to post-process the output data, evaluate it, and make decisions. They can also have algorithms smart enough to process the data and make decisions similar to autonomous vehicles or auto pilot technologies. In this case, a properly functioning SHMS can provide crucial useful information to the public, in a rapid manner; thereby saving a large number of lives. Furthermore, after the earthquake event, data from SHMSs can be used to determine whether or not structures are safe and can be repaired.

What makes a SHMS good?

There are abundant options for creating SHMSs, from types of sensors to network types. Is it wired or wireless? Is it required to perform realtime processing or post-processing? Amid all those variables lies the characteristics of a good SHMS. First, affordability, this can be affected by the structure value as people are willing to pay more to protect expensive or important assets, if we ignore the financial value of human life. Having an affordable system will make it easier to put protecting human life in focus for decision makers such as protecting schools, residential compounds where people usually exist and are not considered as essential or valuable facilities, compared to a company headquarter office or a hospital. In all cases, there’s no meaning of a system that we can’t afford to use.

Next, the reliability of the system which can be viewed from different perspectives such as the ability of the system to function and provide accurate data during the event of interest; which in-turn poses the challenge of power source redundancy for SHMSs. Another aspect of reliability is that the system should be able to wake up from a, possibly long, sleep or stand-by state, perform synchronization if necessary, and start recoding data not missing the event which can be only a few seconds. Redundancy in the SHMS can also be related to the reliability. A possible scenario would be losing connection between system components. Can the components perform off-grid? And once the connection is re-established, can they provide the recorded data during the down time? The answers to such questions can be the difference between obtaining or losing the desired data.

Another important property is the ease of data retrieval from the system. Some SHMSs provide the ability to transmit the data through a mobile-network connection to remote data centers which can be crucial for crisis management. This enables the decision makers to quickly and efficiently focus recovery efforts on the most affected regions. While other systems require either relatively close distance non-contact or even contact data retrieval. The choice between systems can effect priorities when it comes to infrastructure planning to account for possible scenarios.

Other desirable properties of SHMSs are:

- Availability in the market.
- Simplicity and ease of installation, setup, operation and troubleshooting.
- Adaptability to different types of structures such as buildings, bridges, dams, …etc.

Chapter 2

OUTLINE

A study of the latest technology available for use in rapid structural assessment after earthquakes is presented in this thesis. The thesis is divided into two main parts. The first part addresses seismic analysis and includes investigation of the peak floor acceleration-damage relationship while the second part focuses on the literature related to the displacement-damage relationship and the associated latest displacement measuring technology that can be used to assess damage. The background is included for each topic separately in their respective chapters.

In chapter three, the research background regarding peak floor accelerations is discussed along with the importance of this parameter. Then, the modeling approach, analysis procedure, and results of time-history analyses are presented and discussed.

In chapter four, the displacement-damage relationship is introduced by presenting prior research and several methods for obtaining displacements using various instrumentation systems. The potential of digital image correlation is highlighted as a promising low-cost method to measure displacements directly.

Next, in chapter five, limitations of each technique presented in this study are discussed, plus how it would affect its future utilization in a rapid structural inspection system.

Finally, in chapter six, conclusions and future work are presented, and opportunities to build upon this work are discussed.

Chapter 3

PEAK FLOOR ACCELERATION – DAMAGE RELATIONSHIP

3.1 Background

Acceleration is one of the most used parameters in monitoring structures subjected to dynamic loadings. Acceleration can be used directly or to determine other parameters such as velocity and displacement by integrating the signal.

A good example is Shan et al. (2013). They studied the effect of structural story damage on displacement and acceleration at other floors along a building model using a laboratory scale model. A sudden jump in normalized output based on acceleration was observed when damage was introduced. The stiffness change not only gave an indication of the occurrence of damage, but also of its location. (Shan, Yang, Shi, Bridges, & Hansma, 2013).

Accelerometers used to be very expensive, power consuming, large sized and of limited accuracy; however, with the development of Micro-Electro-Mechanical Systems (MEMES), accelerometers are now more affordable, power efficient, small sized and highly accurate. As a result, they are now embedded in many devices around us such as mobile phones and modern cars. The proliferation of low-cost accelerometers has not been seen in structural engineering applications; especially those related to low-cost monitoring of structures in the field. In addition, developing reliable systems that will function for long periods of time, including logging large amount of data while waiting for a major event such as an earthquake to occur, is still a challenge. For this reason, many developers are tending to have devices work in a sleep/awake fashion where a certain threshold is set to trigger recording of the desired parameter.

Other devices are even simpler and can require no power. Those devices, called peak gauges, can retain the single largest value they are subjected to. Back in 2002, in the Advances in Building Technology conference, Mita et al. presented a layout for a device to measure strains using a thin wire that buckles when subject to a certain strain value (Mita & Takahira, 2002). It can be feasible to invest in effort towards interpreting the peak values and thus obtaining useful information. Section 3.9 shows the attempt to interpret peak floor accelerations resulting from time-history analysis of a four, six and eight story building. In this case, the finite element model was reduced to a stick model (as explained in Section 3.3), and then used to obtain the peak values.

Time-history analysis is a valuable way to predict response values for a certain earthquake record. But one can pose the question: How about if we have a new earthquake? Do engineers have to wait for the record to be computerized in order ti run their models to obtain the desired response values? For this reason, many researchers have devoted a great deal of effort in trying to predict the peak values in the first place.

Dynamic analysis has always been simplified using response spectrum where analysts can deal with individual modal responses and then combine them. This case is no exception with small differences. Similar to the one used for design, this approach depends on modal analysis and then modal combination. The latter might add up to the overall error through truncating modes by considering a limited number of modes in the analysis. Researchers have developed methods to overcome this problem such as Pozzi et al. who suggested including the effects of rigid structure (the higher modes) as they are found to contribute considerably to the peak floor acceleration (Pozzi & Kiureghian, 2015).

Modal combination can be done in a variety of ways, the most popular are the CQC and SRSS methods. When they are used to calculate peak displacement, they usually lead to results sufficiently accurate for the purpose of design. However, Taghavi et al. (2006) mentioned that correlation between modal responses has a significant impact on estimating the response if the studied parameter is acceleration. The effect of correlation is found to be higher at lower modes. It is also important to account for correlation between ground motion and modal responses as well, if the absolute acceleration is to be calculated. An extensive study was published by Taghavi-Ardakan et al. (2006) who have worked to develop a method to evaluate the peak floor accelerations using response spectrum. They used a modified version of the CQC method to combine modal responses where modal correlation factors are derived from the power spectral density for actual earthquake records (Taghavi-Ardakan & Miranda, 2006). A summary of the formulas (taken form the source) can be found in Appendix A.1.

Other attempts to evaluate the peak floor acceleration demand in structures followed the work of Taghavi-Ardakan et al. (2006). For example, Moschen et al. (2014) built on Taghavi-Ardakan et al. (2006) and others using a modified CQC combination method. The difference is that cross-correlation coefficients were determined using non-linear regression of previously determined peak floor acceleration values obtained from time-history analysis using a selected earthquake record. A summary of equations taken from the work of Moschen et al. is provided in Appendix A.2.

This can be promising in a way that knowing the normal PFA values of a certain structure subjected to a specific earthquake can help to tell if its behavior is abnormal by comparing those values with measured ones. In Section 03.9 we attempt to find a correlation and/or define a scheme that can distinguish undamaged from damaged structural response.

On the experimental side, it is now possible to get peak acceleration gauges (known commercially as shock gauges) for affordable prices. The primary use of such devices is monitoring valuable packages during shipping and handling by providing a sign if a certain acceleration threshold is crossed. Another option would be wireless sensors network which are available commercially at fairly low prices (around $500 per point at the time of writing this study). These networks can provide a record of acceleration over a limited period of time when triggered by shaking that exceeds a settable threshold.

By collecting peak acceleration data over large areas, it might be possible to attain the goal of identification of a specific geographic area, based on the shared characteristics of structures. Where unusual behavior of structures is observed, careful inspection may be warranted. However, this option is still facing the challenges of reliability, especially at the time of the earthquake event. In addition, the challenge of synchronization for all the devices across the network is discussed in Section 5.2.

3.2 Application: Non-Structural Components

One of the major applications that highlight the importance of peak floor accelerations is the impact on non-structural components. Often times non-structural components have more value than the structure itself. They play the important role of transforming the structure into a functioning building for a targeted use. Those components are usually designed to withstand a certain acceleration limit so that they will remain functioning after the shaking. ASCE 7-10's approach towards designing those components is to design them for a defined amount of force applied at their center of mass. The force depends on a number factors such as spectral acceleration, component type, structural response, and location relatively to the height of the building. This is shown in the following formula quoted from ASCE 7-10 (American Society of Civil Engineers Staff (ASCE), 2013) :

$$F_P = \frac{0.4 a_p S_{DS} W_P}{\left(\frac{R_P}{I_P}\right)} \left(1 + 2\frac{z}{h}\right)$$

Where:

F_P: Seismic design force with a minimum of $1.6 S_{DS} I_P W_P$ and a minimum of $0.3 S_{DS} I_P W_P$

a_p: Component amplification factor that varies from 1.0 to 2.5 (Table 13.5-1 or 13.6-1)

I_P: Component importance factor that varies from 1.0 to 1.5 (Section 13.1.3)

W_P: Component operation weight

R_P: Component response modification factor that varies from 1.0 to 12 (Table 13.5-1 or 13.6-1 ASCE7-10)

z: Height in structure of point of attachment of component with respect to the base. For items at or below the base, z shall be taken as 0. The value of z/h need not to exceed 1.0

h: Average roof height of structure with respect to the base

3.3 Modeling

3.3.1 Building Assumption

In order to study the PFA in a building with various damage states, a building layout has to be assumed. The thought process to develop a “representative” building model started by considering the elastic wind drift limit to approximate a reasonable lateral stiffness. However, the results were excessively stiff models that do not realistically represent current non-engineered construction. Even for the case of engineered buildings, the limit is hardly reached for short buildings, except in some rare cases where wind load is dominant. The next approach attempted involved selecting columns and beams the way people do so when constructing such buildings, by common practice. So, the layout was simply assumed. This assumption is not vital in this stage of the research because as long the relationship between peak acceleration and damage is established, further building layouts can be checked.

The assumed structure was of a four-story residential building with a floor plan shown in Figure 3.1. A grid of 16-inch by 16-inch square concrete columns was use. The columns were connected to beams (10-inches wide by 16-inches deep) and the floor consisted of a 10-inch solid slab was on top of the grid of beams. The assumed floor layout consists of three 20-foot bays in one direction and four 20-foot bays in the other direction. The analysis was carried out considering lateral loading in the 4-bay direction. The story numbering starting from bottom to top with the first floor being the first suspended slab above the ground level.

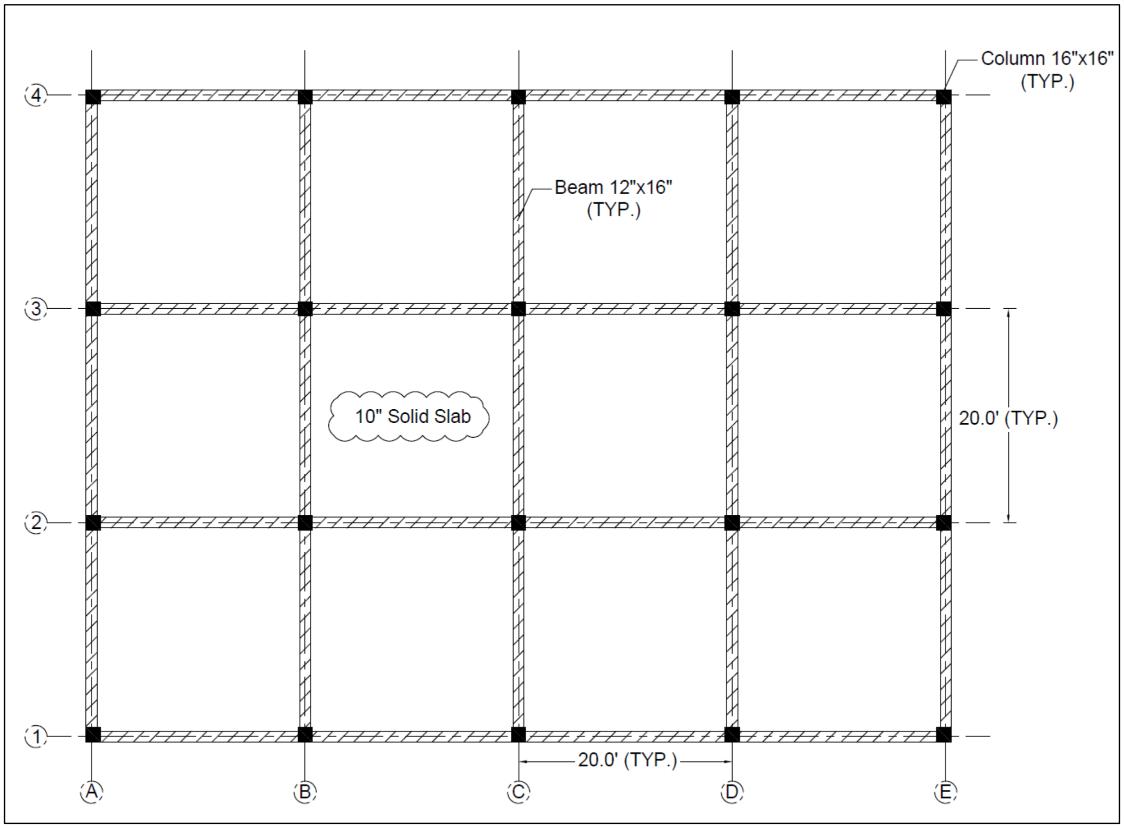

Figure 3.1 Assumed floor plan

Columns dimensions were assumed based on short column gravity loading. Beams and slabs were simply assumed as well as the concrete material properties which were set to be 4,000 psi concrete with grade 60 rebar. This layout was selected because it resembles the case of many residential buildings in developing countries such as Jordan, where people inhabiting such non-engineered buildings come from low income populations for which this research is aimed to support.

The structural system was assumed to be an ordinary concrete moment resisting frame. Although it is not commonly used in these buildings, the simplicity in interpreting the results made it a good choice to start with. In future, the complexities of including shear walls or even dual systems can be added. The floor loads were calculated according to ASCE 7-10 with the assumptions summarized in Table 3.1 (American Society of Civil Engineers Staff (ASCE), 2013).

Table 3.1 Load assumptions (a) Area loads, (b) Line loads

(a)

Item	Load (psf)	Notes
Finish	16	Ceramic finish, ASCE-7 10 Table C3-1
MEP	10.4	ASCE-7 10 Table C3-1
Live Load	40	ASCE-7 10 Table 4-1

(b)

Item	Load (lb/ft)	Notes
Exterior Walls Equiv.	290	6-inch Hollow concrete wythes - No grout + 2 faces plaster, ASCE-7 10 Table C3-1
Interior Walls Equiv.	270	4-inch Hollow concrete wythes - No grout + 2 faces plaster, ASCE-7 10 Table C3-1

3.3.2 Analysis Procedure

A linear time-history analysis procedure was selected because it enables simulation of a realistic earthquake record and yields response with respect to time at each floor level. With the time-history response in hand, the peak values can be identified with confidence. The selection of the linear elastic approach was made for simplicity. Future work could introduce nonlinearity into the analysis to better estimate the structural response.

A full 3D finite element model was created for the assumed building. To reduce the considerable computational effort, it was then reduced to a stick model (lumped mass model) representing the one direction of loading.

The process of creating the stick model was according to the following assumptions (see summary in Figure 3.2).

- Mass of every story was lumped into a single node.
- All vertical elements were assumed to be a single column connecting lumped mass nodes.
- The base constraint is assumed to be fixed for all models.
- The stiffness for the stick model was determined as follows:
    1. Assuming rigid floor for the full 3D model and adjusting vertical element stiffness in the stick model to match displacements and frequencies of the full 3D model with rigid floors.
    2. Adding rotational springs at each node of the stick model to represent floor stiffness, then adjusting the rotational spring stiffnesses to match responses of the full 3D model without the rigid floor constraint but including restrains on the diaphragm in-plane deformation.

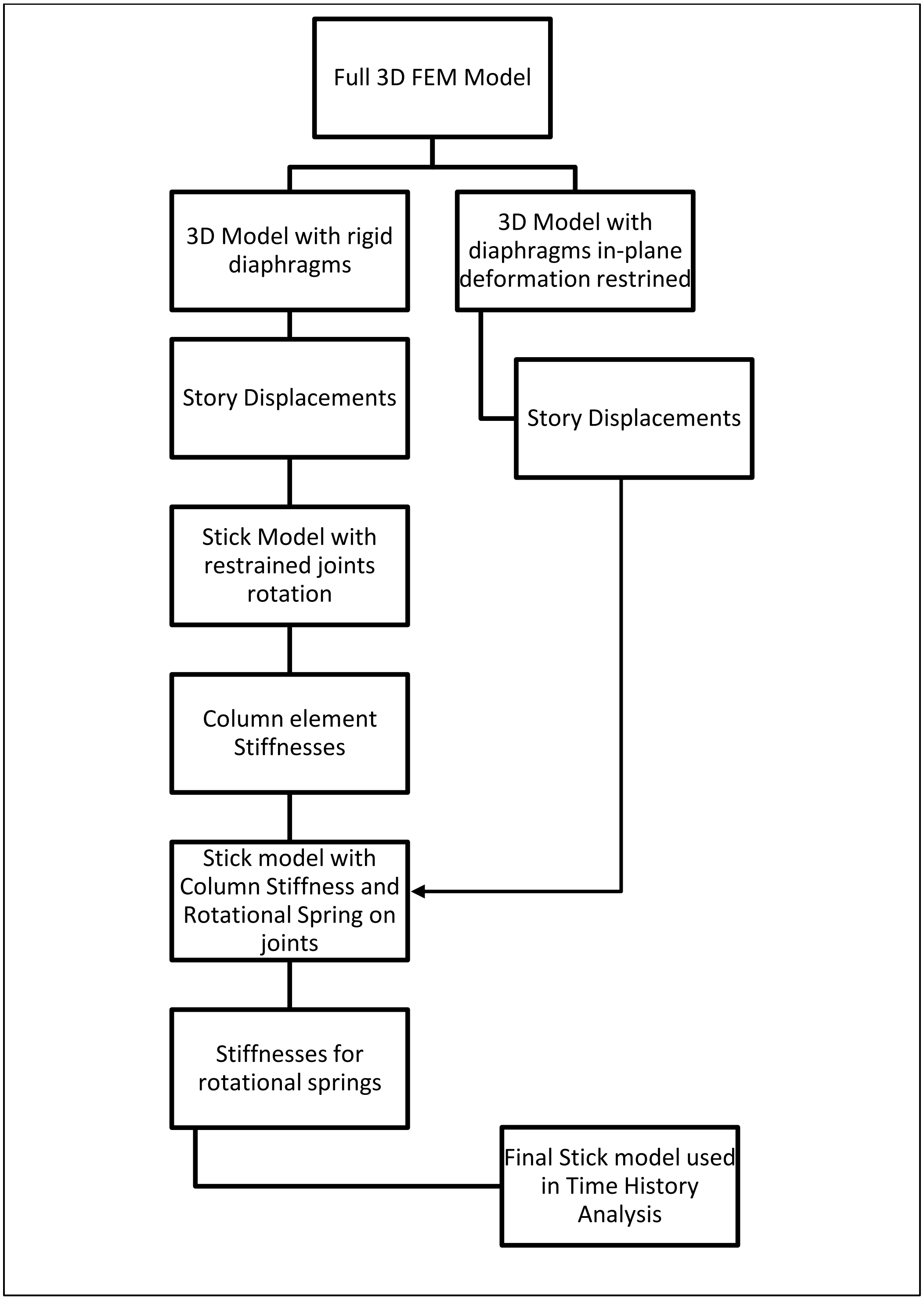

Figure 3.2 Stick model development process

The result is a simplified model that can represent the full 3D model's behavior and give approximate responses without the need for performing analysis on the full 3D model each time; which saves time and computational effort.

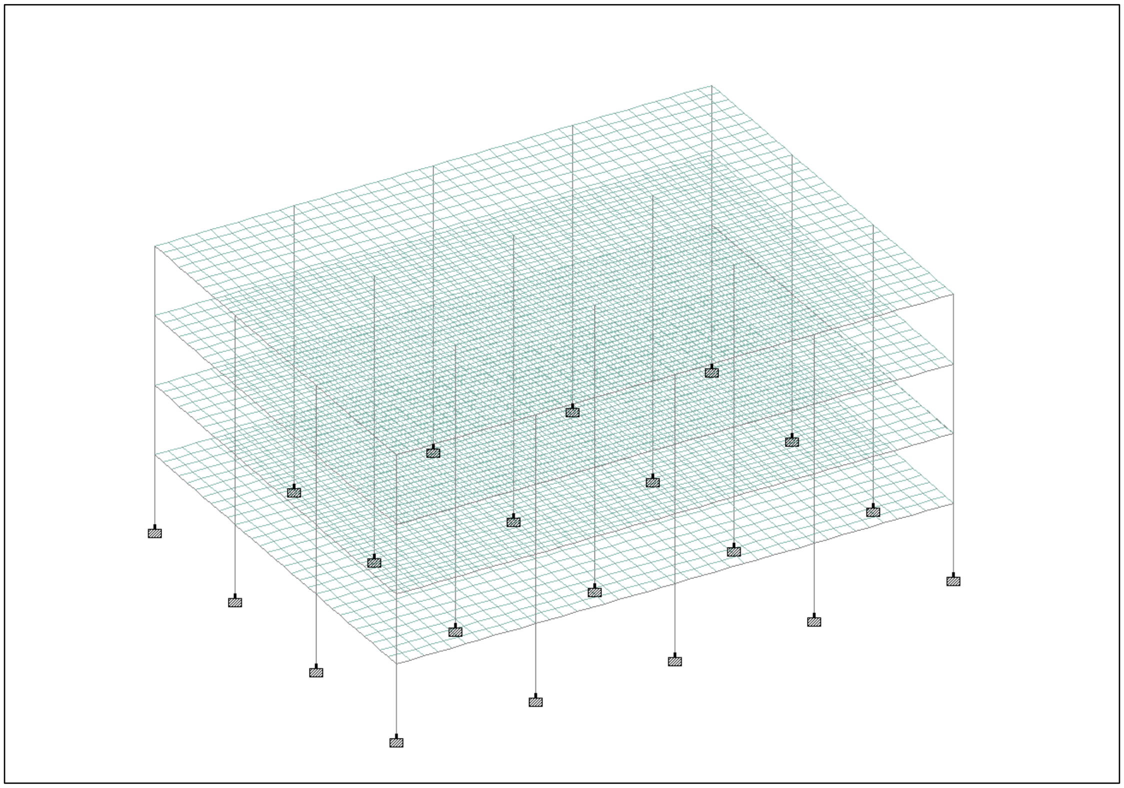

Figure 3.3 Full 3D finite element model using STAAD Pro.

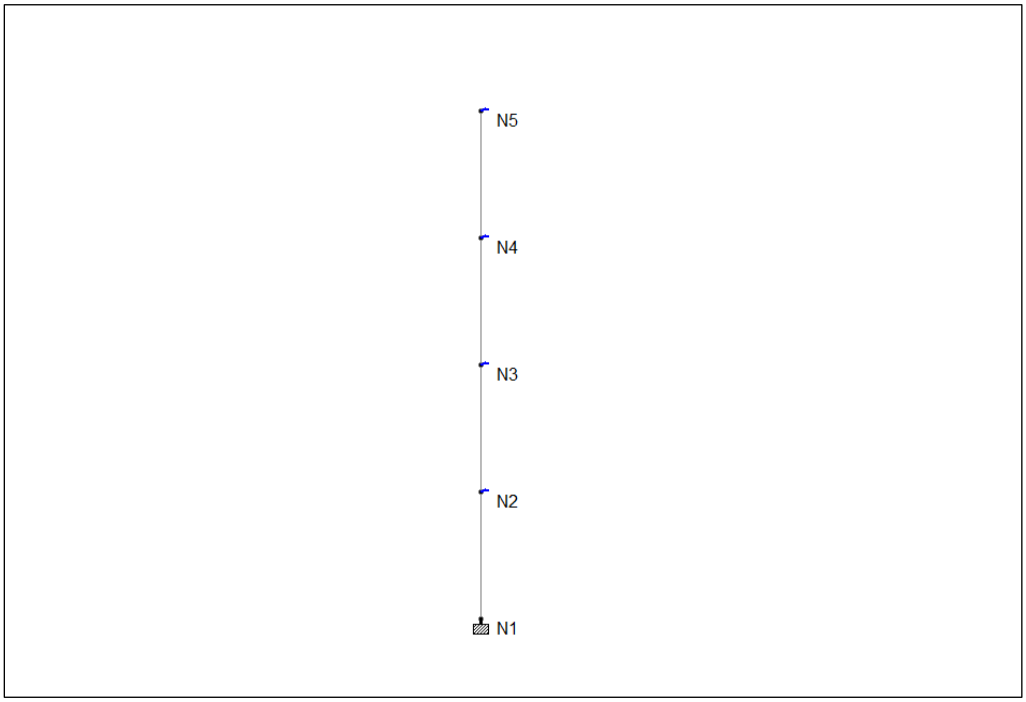

Figure 3.4 Simplified stick model

To verify the stick model, modal analysis was carried out and the structural periods were compared with the corresponding periods from the full 3D model (see Table 3.2).

Table 3.2 Stick model verification - Structural period

Mode	Period		
	Full 3D Model	Stick Model	Error
#	s	s	
1	2.687	2.687	0.00%
2	0.863	0.865	0.23%
3	0.497	0.5	0.60%
4	0.363	0.365	0.55%

Both models were then subjected to Mexico earthquake record (as per Table 3.4). The resulting peak accelerations matching each other very well as shown in Table 3.3 .

Table 3.3 Peak floor acceleration results from stick model versus the full 3D model

Story	Peak Floor Acceleration		
	Full 3D Model	Stick Model	Error
#	in/s²	in/s²	
1	18.8	18.5	-1.5957%
2	29.5	29.3	-0.6780%
3	33	33	0.0000%
4	44.1	44.4	0.6803%

After ensuring that the stick model had very similar behavior in terms of peak floor accelerations, it was used to perform a complete time-history analysis. Multiple earthquake records were applied to the base and peak acceleration responses were noted at each floor level.

3.3.3 Damage Idealization

In this study damage was idealized as a reduction in the moment of inertia of the columns. Although in reality the damage might take on a more complex nature, this assumption was made to simplify the analysis since the lateral stiffness is directly related to the moment of inertia of the columns.

First, the undamaged state was considered to be represented by the gross moment of inertia for the columns. Then, damage was introduced to the first-floor columns. The reason behind introducing damage to the first floor is that for a uniform stiffness building, the vulnerability of the first level is higher as they suffer the maximum story shear with a similar strength to other stories. Two states of damage were considered and were represented by 25% and 50% reduction in inertia. Next, the location where the damaged columns are assumed is switched from the first floor to the third floor in order to evaluate the effect of damage of a floor that is neither the uppermost nor the lowermost floor.

Linear time-history analysis using STAAD.Pro V8i yielded the full response of each state with respect to time. Maximum acceleration at each floor level (peak floor acceleration, PFA) was recorded for each case and the results are summarized in Section 3.4.

3.3.4 Ground Motion Records

Multiple ground motion records were obtained from the CSMIP (California Strong Motion Program) website (https://strongmotioncenter.org/). These records represent a number of recent major earthquakes. The records used in this study are shown in Table 3.4. The ID column represent the name with which each record is referred to throughout this study.

Table 3.4 Earthquake records used

ID	Month Year	Station	Mag.	PGA (g)	Channel
El Centro	May 1940	Imperial Valley, Station NO. 117, CA	6.9	0.359	S00E
Mexico	Sep. 2017	Unam - Mexico, Mexico	7.1	0.055	HNE
Chile (Valparaiso)	Apr. 2017	Torpederas, Chile	6.9	0.906	HNE
New Zealand (Amberley)	Nov. 2016	Ward Fire Station, New Zealand	7.8	1.279	HS12E

3.4 Results: Peak Floor Accelerations

In this section, results are shown for the time-history analysis performed on the four-story building. Peak floor accelerations corresponding to the three assumed damage states (undamaged, 25% damage, and 50% damage), for the first floor damage case (see Section3.4.1) and the third floor damage case (see Section 3.4.2), are shown in Tables 3-5 and 3-6 and Figures 3-5 and 3-6.

3.4.1 First Floor Damage

Table 3.5 PFA (in/s^2) corresponding to damage percentage of vertical elements at first floor for (a) El Centro EQ (b) Mexico EQ (c) Chile EQ (d) New Zealand EQ

(a)

Damage State	Undamaged	25%	50%
Story	in/s^2	in/s^2	in/s^2
4	344	354	317
3	313	320	313
2	283	280	310
1	214	211	219
0	0	0	0

(b)

Damage State	Undamaged	25%	50%
Story	in/s^2	in/s^2	in/s^2
4	41.9	46.8	49.8
3	34	44.1	38
2	30.4	38.2	32.6
1	17.7	28.2	25
0	0	0	0

(c)

Damage State	Undamaged	25%	50%
Story	in/s^2	in/s^2	in/s^2
4	399	354	323
3	364	341	363
2	575	379	415
1	529	384	434
0	0	0	0

Table 3.5 continued

(d)

Damage State	Undamaged	25%	50%
Story	in/s^2	in/s^2	in/s^2
4	343	350	405
3	366	340	417
2	407	350	446
1	363	374	422
0	0	0	0

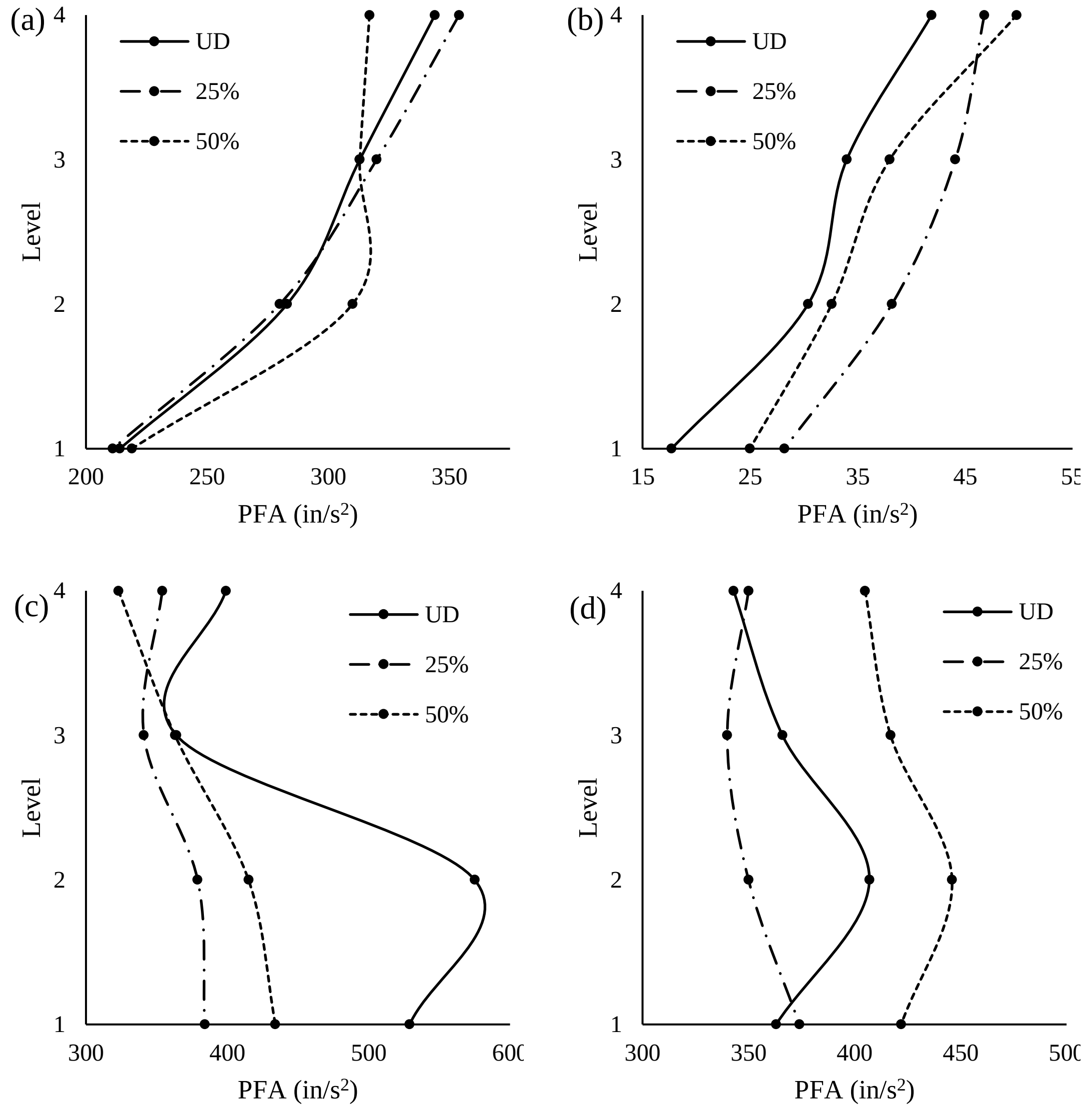

Figure 3.5 PFA for four story building with the damage induced on the first story for (a) El Centro EQ (b) Mexico EQ (c) Chile EQ (d) New Zealand EQ

3.4.2 Third Floor Assumed Damage:

Table 3.6 PFA (in/s^2) corresponding to damage percentage of vertical elements at third floor for (a) El Centro EQ (b) Mexico EQ (c) Chile EQ (d) New Zealand EQ

(a)

Damage State	Undamaged	25%	50%
Story	in/s^2	in/s^2	in/s^2
4	344	351	366
3	313	327	317
2	283	278	278
1	214	219	230
0	0	0	0

(b)

Damage State	Undamaged	25%	50%
Story	in/s^2	in/s^2	in/s^2
4	41.9	45.1	48.7
3	34	38.4	40.4
2	30.4	41.4	39.1
1	17.7	24	22.9
0	0	0	0

(c)

Damage State	Undamaged	25%	50%
Story	in/s^2	in/s^2	in/s^2
4	399	321	339
3	364	360	360
2	575	418	471
1	529	555	517
0	0	0	0

Table 3.6 continued

(d)

Damage State	Undamaged	25%	50%
Story	in/s^2	in/s^2	in/s^2
4	343	390	370
3	366	406	423
2	407	428	445
1	363	442	425
0	0	0	0

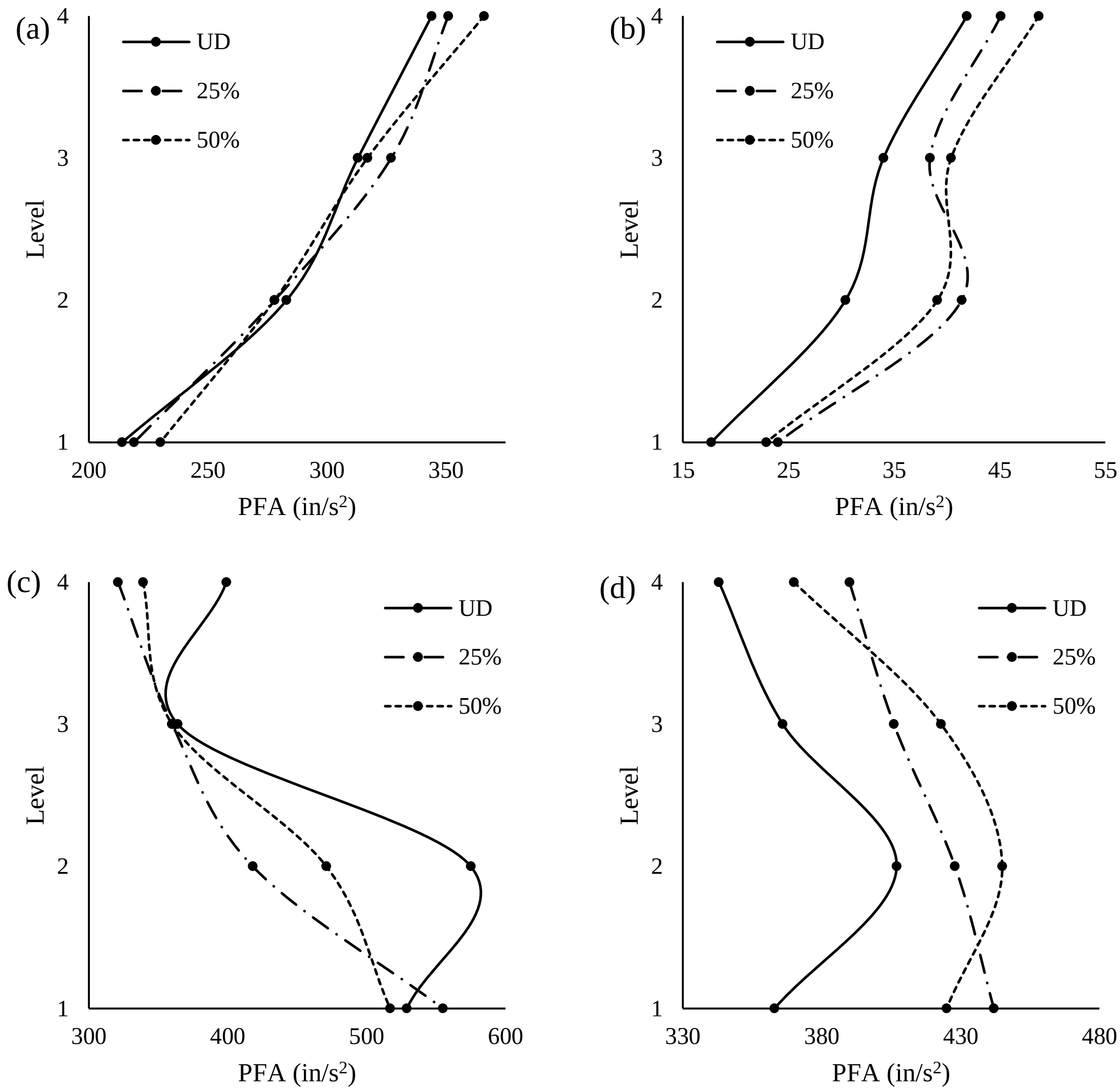

Figure 3.6 PFA for four story building with the damage induced on the third story for (a) El Centro EQ (b) Mexico EQ (c) Chile EQ (d) New Zealand EQ

3.5 Variance Calculation

In order to measure the spread of the PFA along the building, the variance was calculated for relative peak floor acceleration in each case: undamaged model, damage assumed to the first floor 25% and 50% and damage assumed to the third floor 25% and 50% using the following formula and the data from Section 3.4:

$$VAR = \frac{\sum_{i=1}^{n}\left[\left(a_i - a_{avg}\right)^2\right]}{n-1}$$

Where:

VAR : Variance for absolute PFA along the building height

a_i : Absolute PFA for floor i

a_{avg} : Average absolute PFA along the building height

n : Number of floor levels

3.5.1 Variance Calculation for The First-Floor Damage Case

The following tables show the variance calculation process for inter-story absolute peak acceleration.

Table 3.7 PFA variance calculation assuming damage is in first floor for (a) El Centro EQ (b) Mexico EQ (c) Chile EQ (d) New Zealand EQ

(a)

Damage State	Undamaged	25%	50%
Story	$(a-a_{avg})^2$	$(a-a_{avg})^2$	$(a-a_{avg})^2$
4	3080.3	3937.6	742.6
3	600.3	826.6	540.6
2	30.3	126.6	410.1
1	5550.3	6440.1	5005.6
0	0.0	0.0	0.0
Variance	3087.0	3776.9	2232.9

(b)

Damage State	Undamaged	25%	50%
Story	$(a-a_{avg})^2$	$(a-a_{avg})^2$	$(a-a_{avg})^2$
4	118.8	55.9	180.9
3	9.0	22.8	2.7
2	0.4	1.3	14.1
1	176.9	123.8	128.8
0	0	0	0
Variance	101.7	67.9	108.8

(c)

Damage State	Undamaged	25%	50%
Story	$(a-a_{avg})^2$	$(a-a_{avg})^2$	$(a-a_{avg})^2$
4	4590.1	110.3	3690.6
3	10557.6	552.3	430.6
2	11718.1	210.3	976.6
1	3875.1	380.3	2525.1
0	0	0	0
Variance	10246.9	417.7	2540.9

Table 3.7 continued

(d)

Damage State	Undamaged	25%	50%
Story	$(a-a_{avg})^2$	$(a-a_{avg})^2$	$(a-a_{avg})^2$
4	715.6	12.3	306.3
3	14.1	182.3	30.3
2	1387.6	12.3	552.3
1	45.6	420.3	0.3
0	0	0	0
Variance	720.9	209.0	296.3

Table 3.8 Variance comparison: First floor damage

Damage	El Centro	Mexico	Chile	New Zealand
0%	3087	102	10247	721
25%	3777	68	418	209
50%	2233	109	2541	296

Table 3.9 Variance change percentage: First floor damage

Damage	El Centro	Mexico	Chile	New Zealand
0%	0%	0.0%	0.0%	0.0%
25%	22%	-33.2%	-95.9%	-71.0%
50%	-28%	7.0%	-75.2%	-58.9%

Figure 3.7 illustrates how the variance of PFA changes with damage percentage for the first story for each earthquake record.

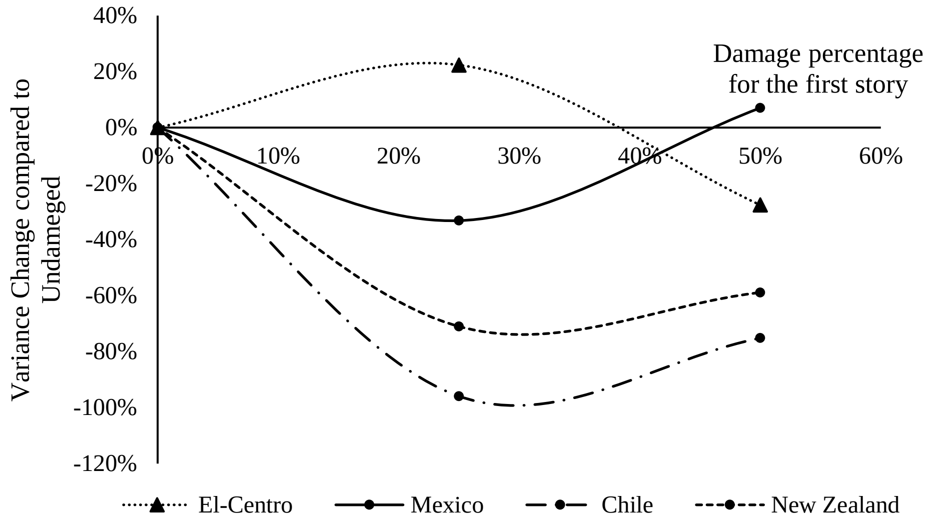

Figure 3.7 Change in PFA variance with damage of the first floor

3.5.2 Variance Calculation for The Third-Floor Damage Case

Table 3.10 PFA variance calculation assuming damage is in first floor for (a) El Centro EQ (b) Mexico EQ (c) Chile EQ (d) New Zealand EQ

(a)

Damage State	Undamaged	25%	50%
Story	$(a-a_{avg})^2$	$(a-a_{avg})^2$	$(a-a_{avg})^2$
4	3080.3	3277.6	4658.1
3	600.3	1105.6	370.6
2	30.3	248.1	390.1
1	5550.3	5587.6	4590.1
0	0.0	0.0	0.0
Variance	3087.0	3406.3	3336.3

Table 3.10 continued

(b)

Damage State	Undamaged	25%	50%
Story	$(a-a_{avg})^2$	$(a-a_{avg})^2$	$(a-a_{avg})^2$
4	118.8	62.0	119.4
3	9.0	1.4	6.9
2	0.4	17.4	1.8
1	176.9	174.9	221.3
0	0.0	0.0	0.0
Variance	101.7	85.2	116.4

(c)

Damage State	Undamaged	25%	50%
Story	$(a-a_{avg})^2$	$(a-a_{avg})^2$	$(a-a_{avg})^2$
4	4590.1	8556.3	6847.6
3	10557.6	2862.3	3813.1
2	11718.1	20.3	2425.6
1	3875.1	20022.3	9072.6
0	0.0	0.0	0.0
Variance	10246.9	10487.0	7386.3

(d)

Damage State	Undamaged	25%	50%
Story	$(a-a_{avg})^2$	$(a-a_{avg})^2$	$(a-a_{avg})^2$
4	715.6	702.3	2093.1
3	14.1	110.3	52.6
2	1387.6	132.3	855.6
1	45.6	650.3	85.6
0	0.0	0.0	0.0
Variance	720.9	531.7	1028.9

Table 3.11 Variance comparison: Third floor damage

Damage	El Centro	Mexico	Chile	New Zealand
0%	3087	102	10247	721
25%	3406	85	10487	532
50%	3336	116	7386	1029

Table 3.12 Variance change percentage: Third floor damage

Damage	El Centro	Mexico	Chile	New Zealand
0%	0.0%	0.0%	0.0%	0.0%
25%	10.3%	-16.2%	2.3%	-26.3%
50%	8.1%	14.5%	-27.9%	42.7%

Figure 3.8 illustrates the how the variance of PFA changes with damage percentage for the third story for each earthquake record.

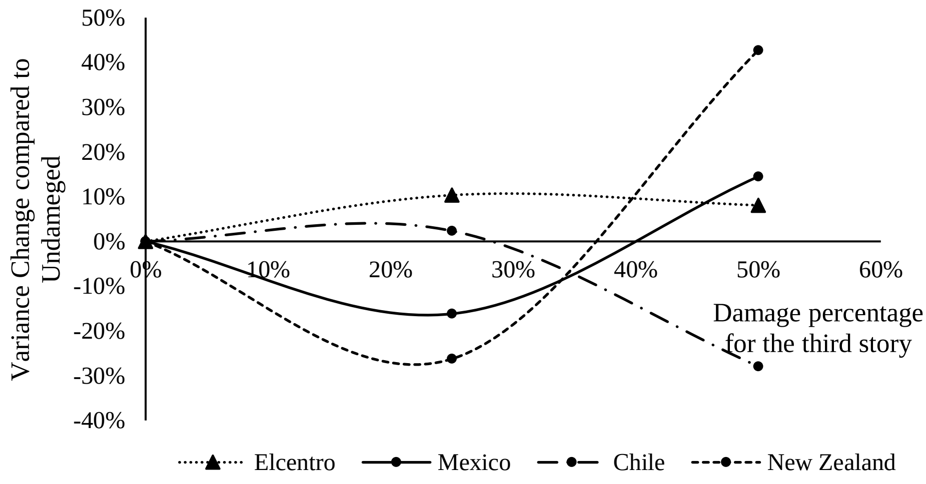

Figure 3.8 Change in PFA variance with damage of the third floor

3.6 Considering Different Buildings Heights

Up until now we have only considered one building height. At this point, we will consider buildings of different height being subjected to the same earthquake records. This will allow us to see whether a pattern can be identified with the height of the buildings. To start with a simple case, a uniform stiffness scenario was considered by replicating the four-story building into six and eight story models. Although in real life the designer would increase the size of columns in the lower floors, the simple case was taken as a starting point. Then, to represent a practical case, columns sizes were increased in the lower stories of the six and eight stories models as shown in Table 3.13. The results of both scenarios were then summarized in the Figures 3.9 through 3.14. In all cases covered in this section, damage was assumed to take place in the only the first floor. All values used to plot the figures are included in Appendix B. Finally, variance was calculated using the same procedure described earlier.

Table 3.13   Non-uniform stiffness models column sizes

	Square Column Side Length (in.)		
Floors	4S	6S	8S
1-2	16	18	20
3-4	16	16	18
5-6	-	16	16
7-8	-	-	16

3.6.1 Uniform Stiffness Model

3.6.1.1 PFA Profile for Uniform Stiffness Six Stories Building

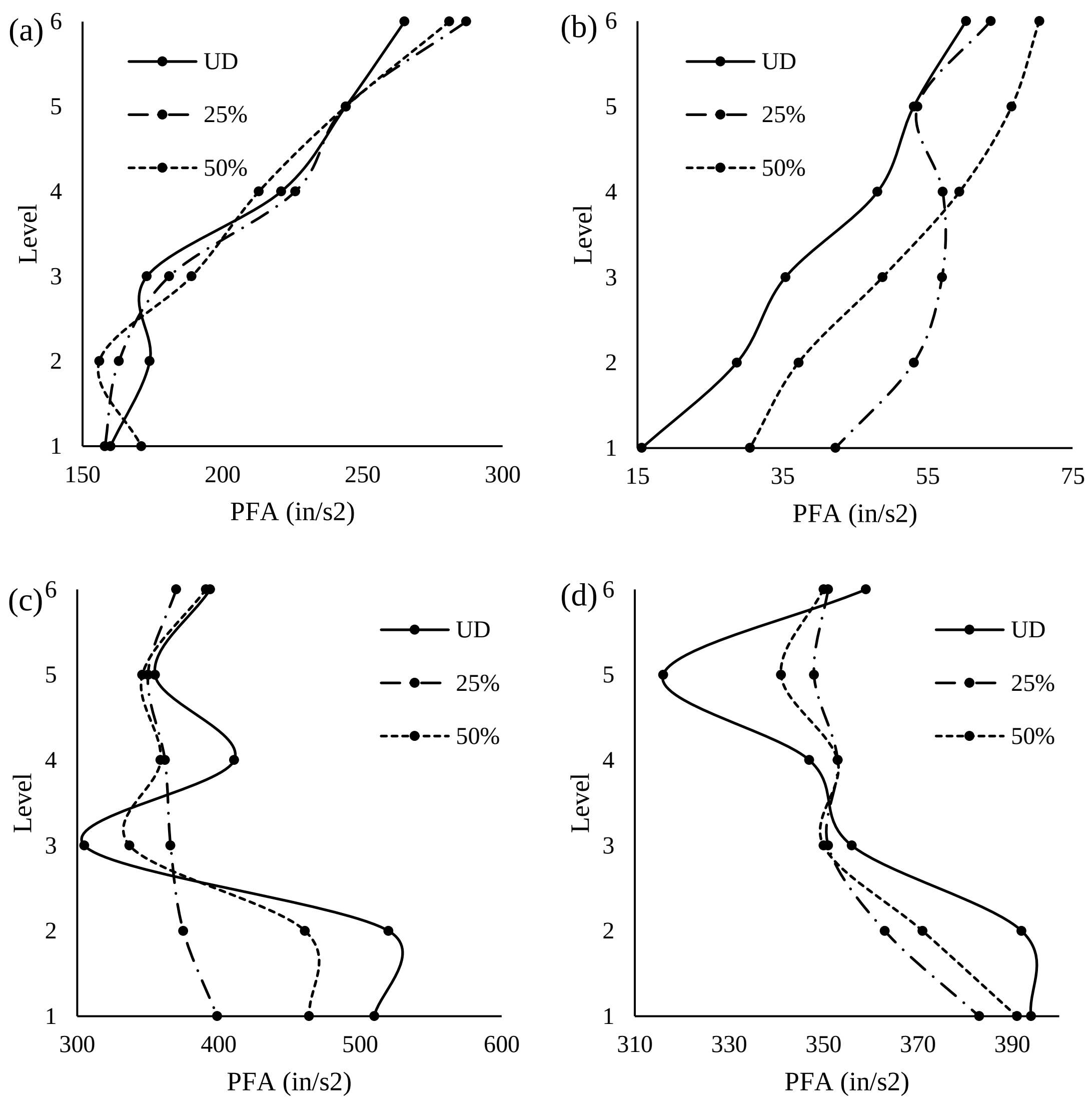

Figure 3.9 PFA for six story uniform stiffness building with the damage induced on the first story for (a) El Centro EQ (b) Mexico EQ (c) Chile EQ (d) New Zealand EQ

3.6.1.2 PFA Profile for Uniform Stiffness Eight Stories Building

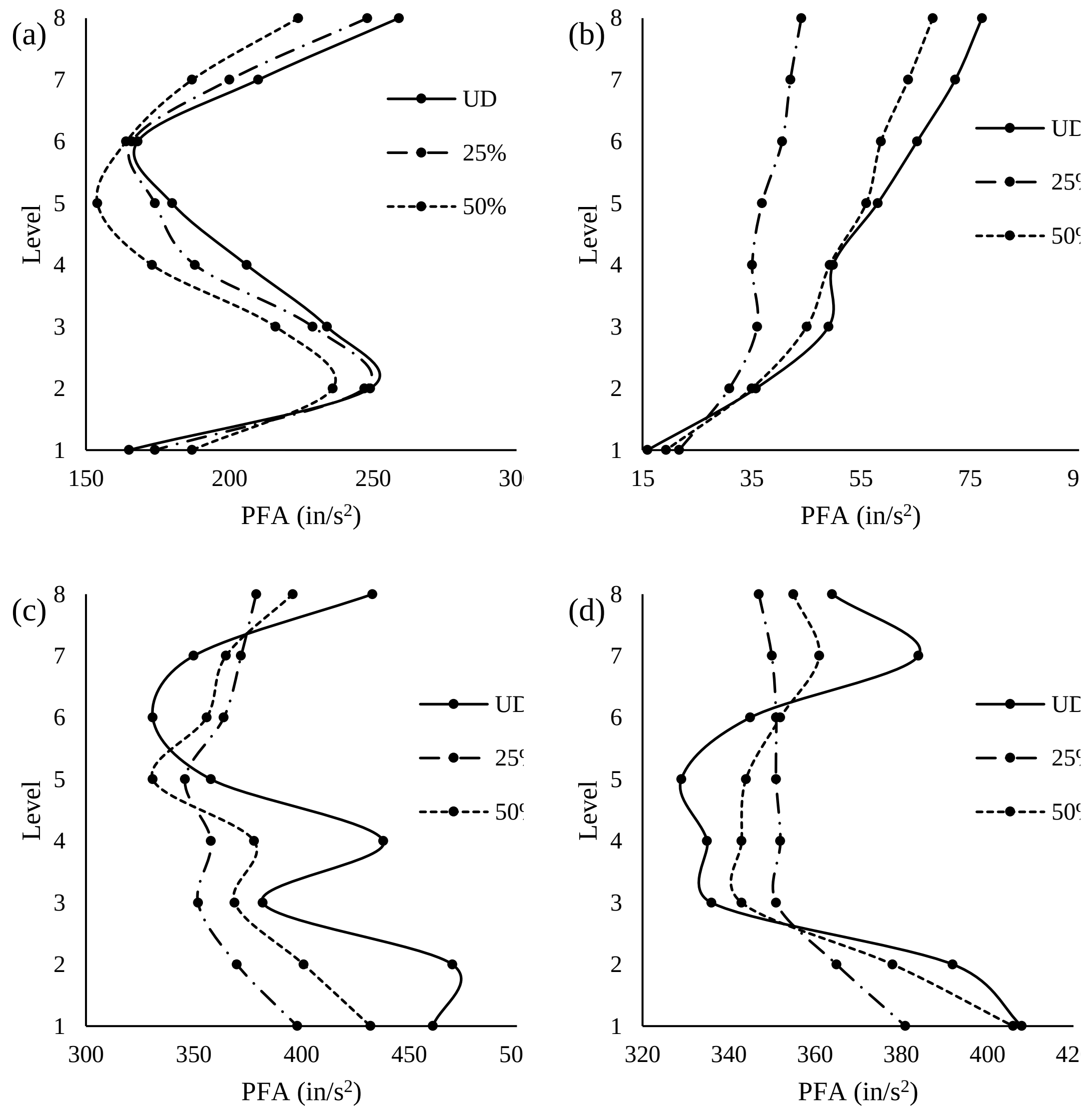

Figure 3.10 PFA for eight story uniform stiffness building with the damage induced on the first story for (a) El Centro EQ (b) Mexico EQ (c) Chile EQ (d) New Zealand EQ

3.6.1.3 Variance Calculation for Uniform Stiffens Building Response

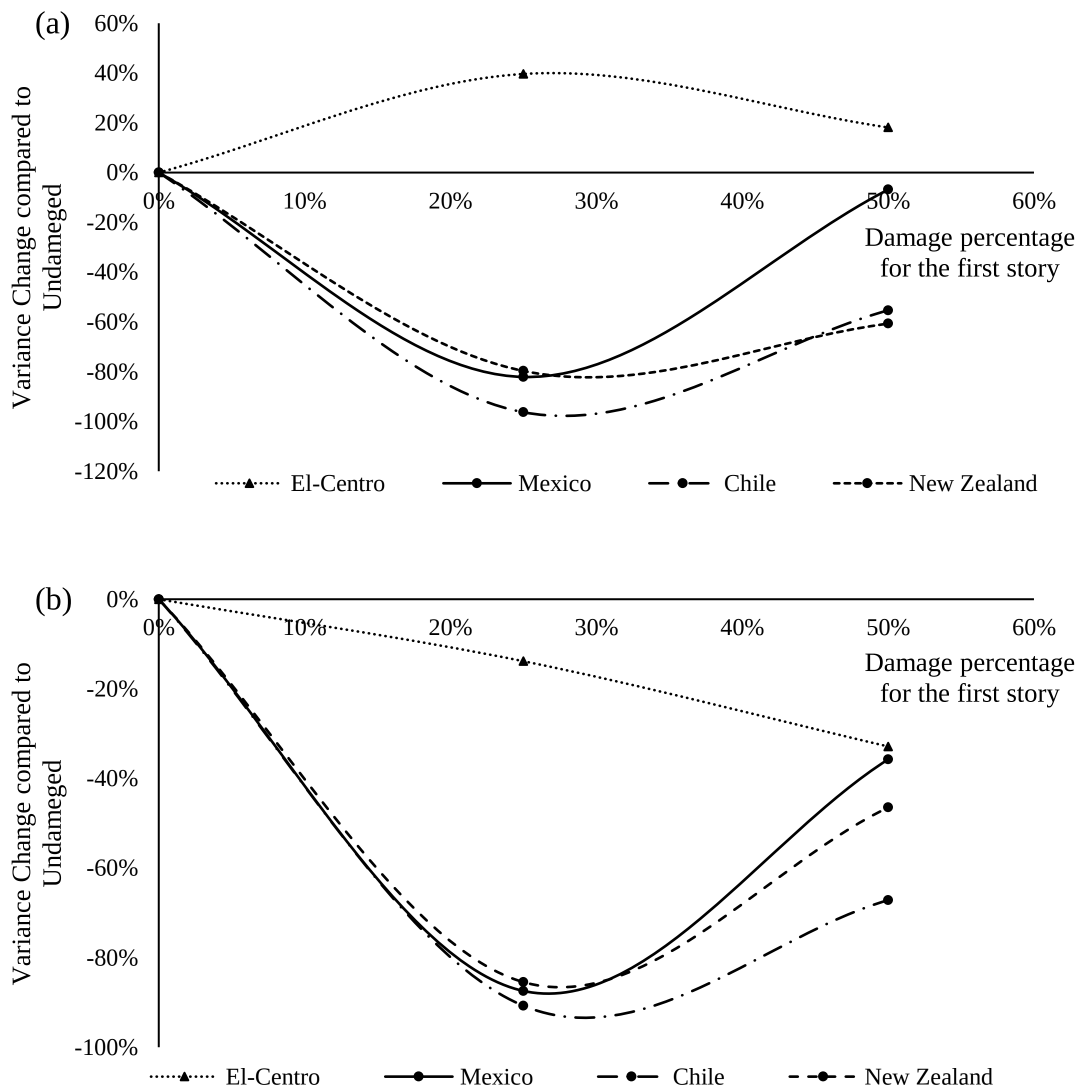

Figure 3.11 Variance in PFA change with damage induced on the first story for uniform stiffness building (a) Six story building (b) Eight story building

3.6.2 Non-Uniform Stiffness Model

3.6.2.1 PFA Profile for Non-Uniform Stiffness Six Stories Building

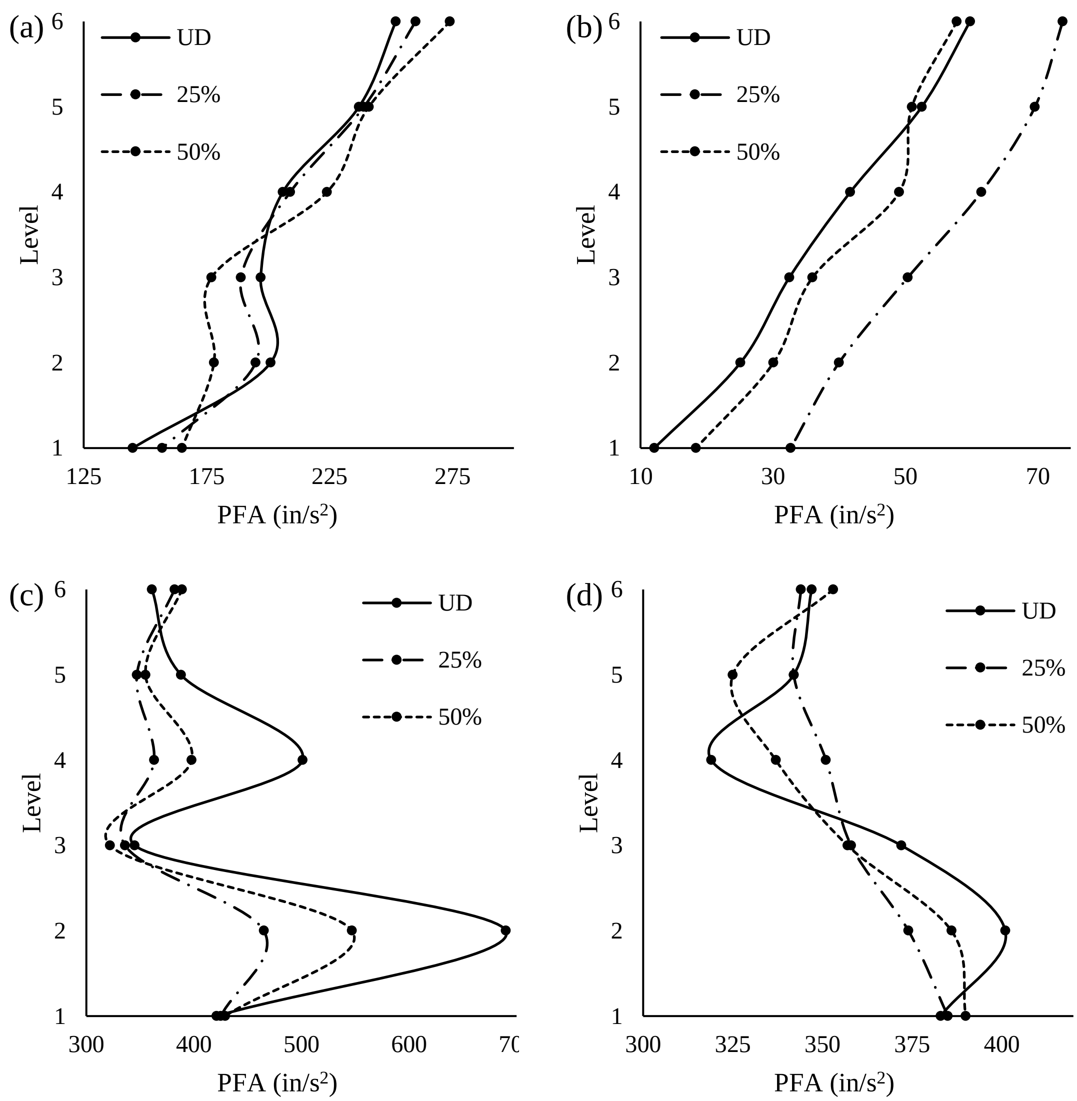

Figure 3.12 PFA for six story non-uniform stiffness building with the damage induced on the first story (b) Mexico EQ (c) Chile EQ (d) New Zealand EQ

3.6.2.2 PFA Profile for Non-Uniform Stiffness Eight Stories Building

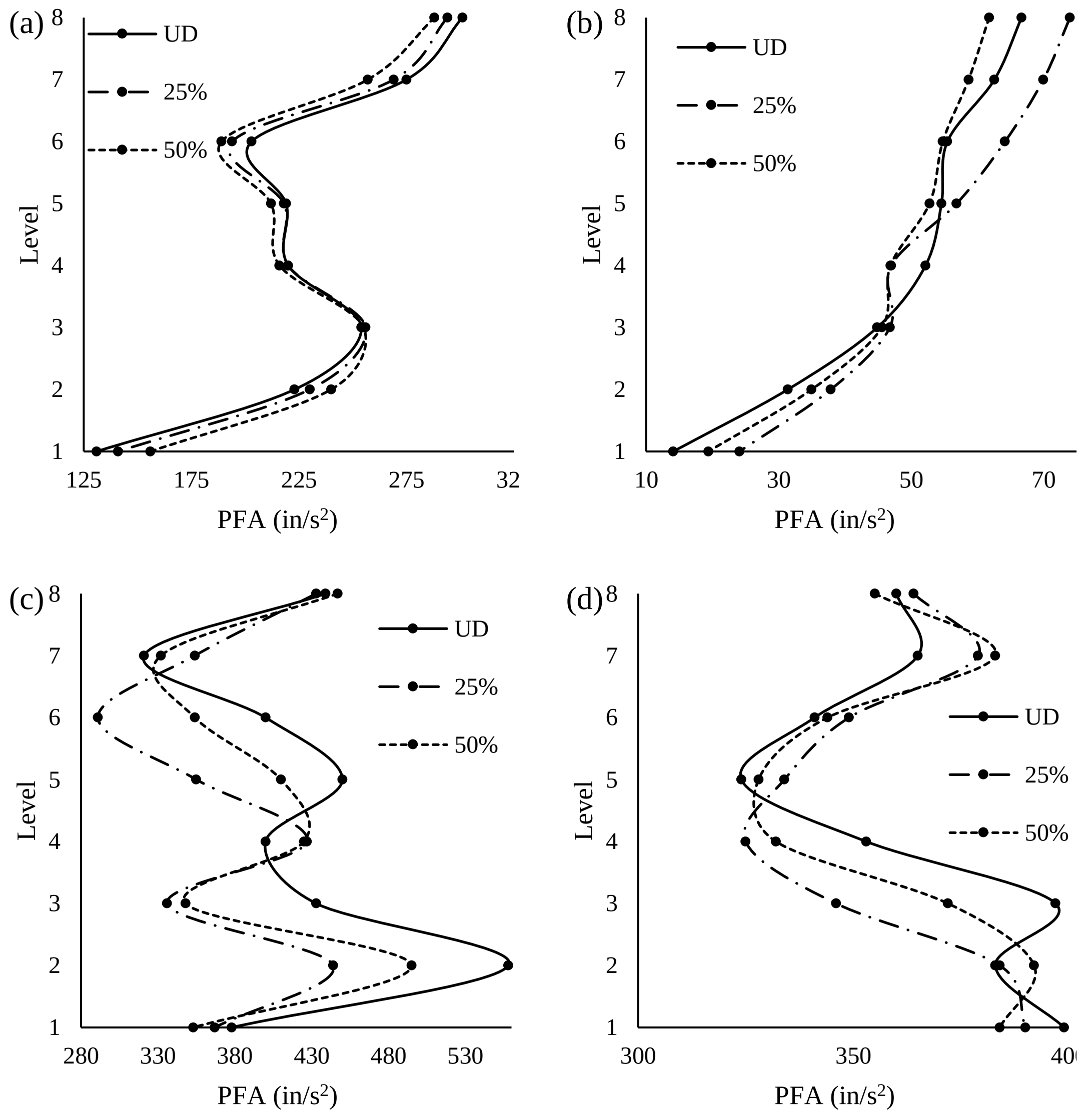

Figure 3.13 PFA for eight story non-uniform stiffness building with the damage induced on the first story (b) Mexico EQ (c) Chile EQ (d) New Zealand EQ

3.6.2.3 Variance Calculation for Non-Uniform Stiffens Building Response

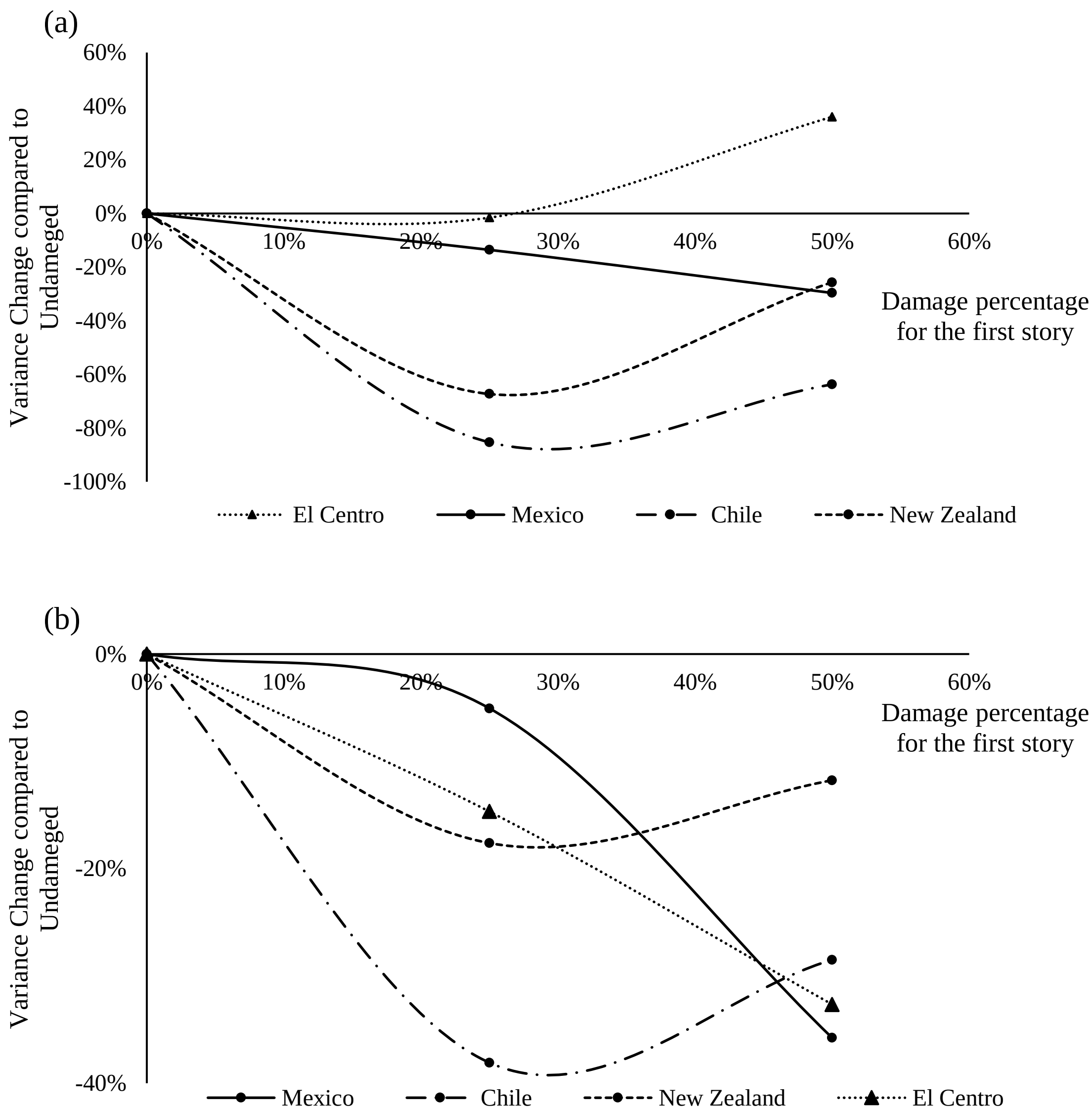

Figure 3.14 Variance in PFA change with damage induced on the first story for non-uniform stiffness building (a) Six story building (b) Eight story building

3.7 Change in PFA Profile Due to Damage for Uniform Stiffness Buildings

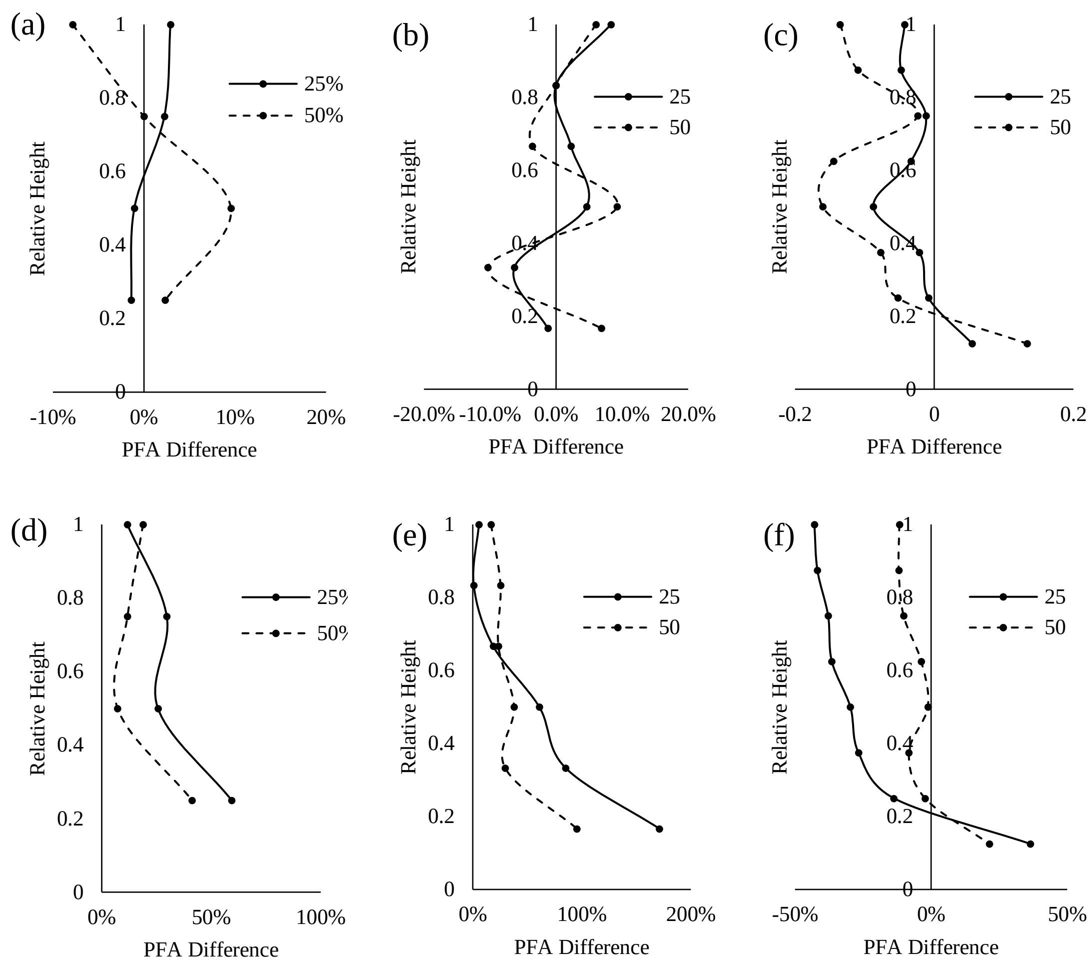

Figure 3.15 Change of PFA profile due to damage relative to the undamaged state for (a, b and c) El Centro EQ (d, e and f) Mexico EQ (g, h and i) Chile EQ (j, k and l) New Zealand EQ for four, six and eight story respectively with uniform stiffness

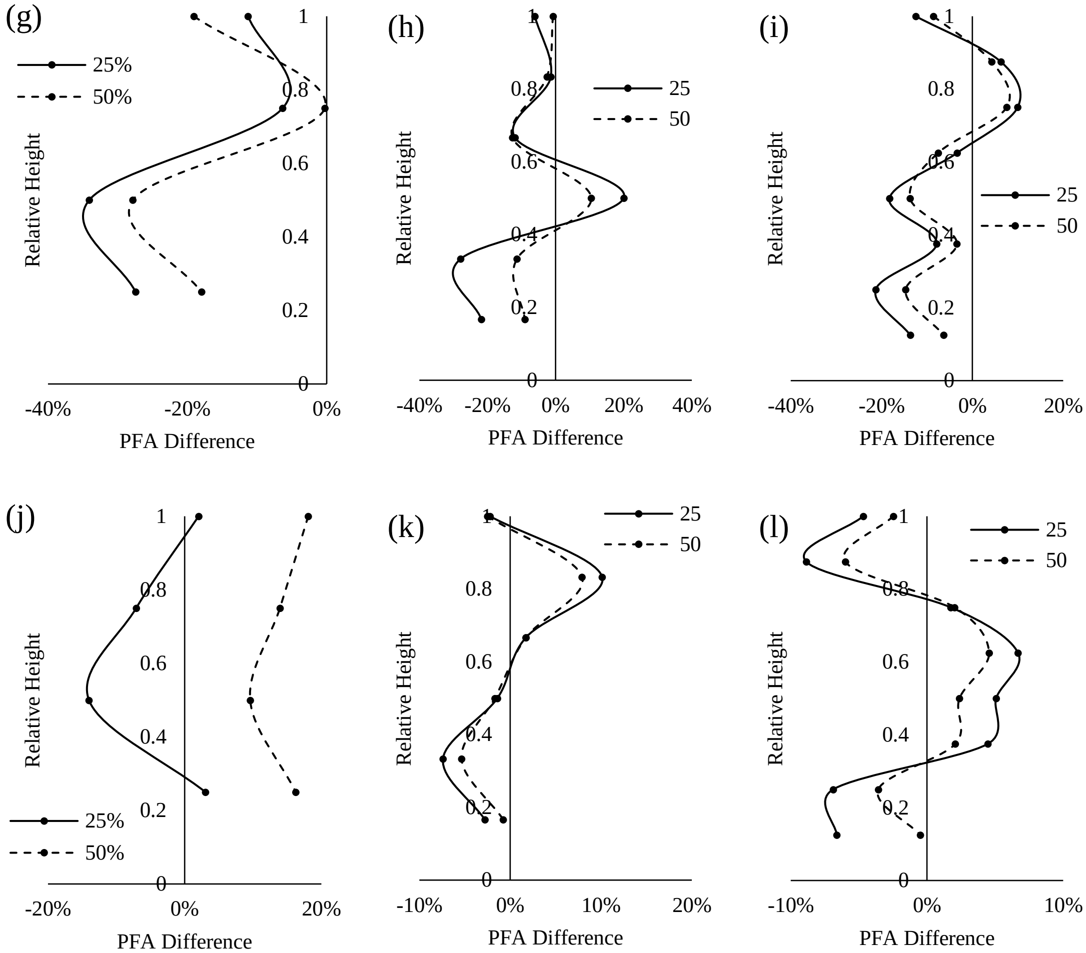

Figure 3.15 continued

3.8 Change in PFA Profile Due to Damage for Non-Uniform Stiffness Buildings

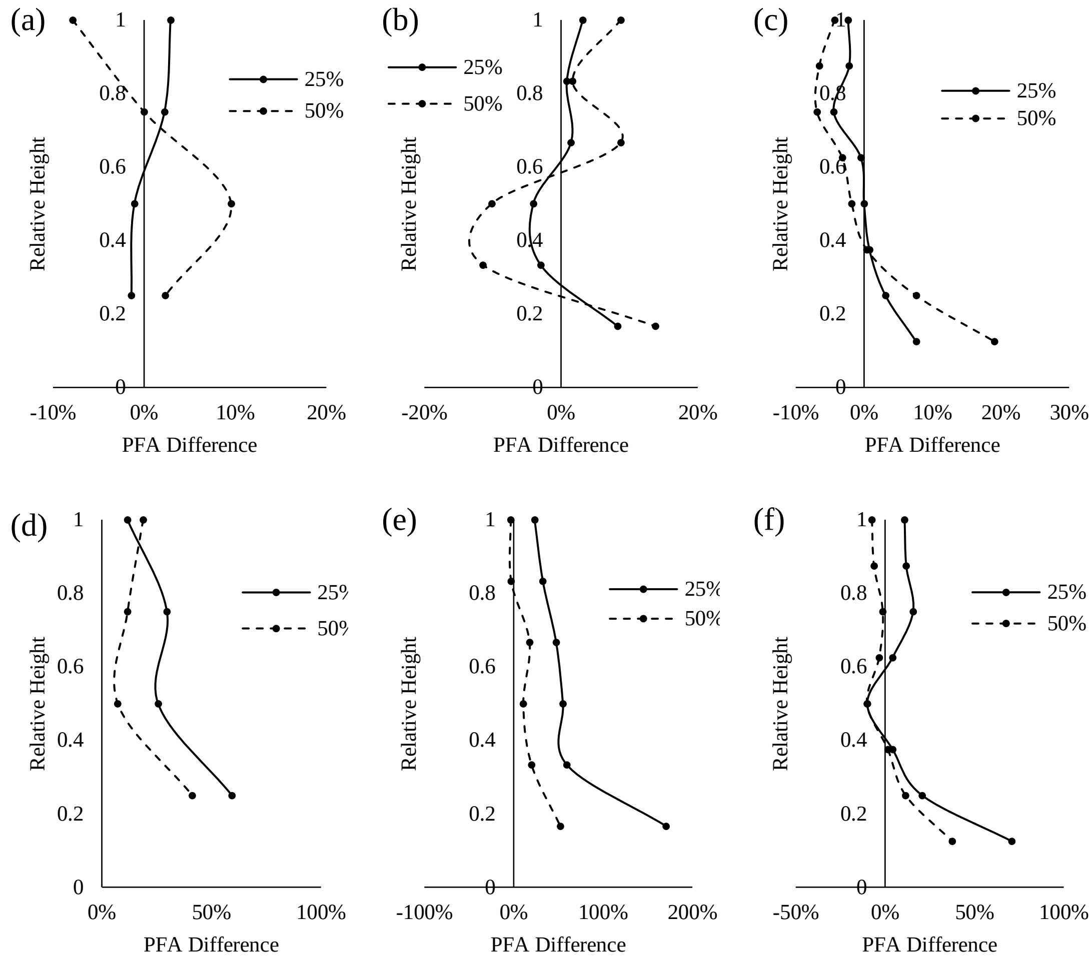

Figure 3.16 Change of PFA profile due to damage relative to the undamaged state for (a, b and c) El Centro EQ (d, e and f) Mexico EQ (g, h and i) Chile EQ (j, k and l) New Zealand EQ for four, six and eight story respectively with non-uniform stiffness

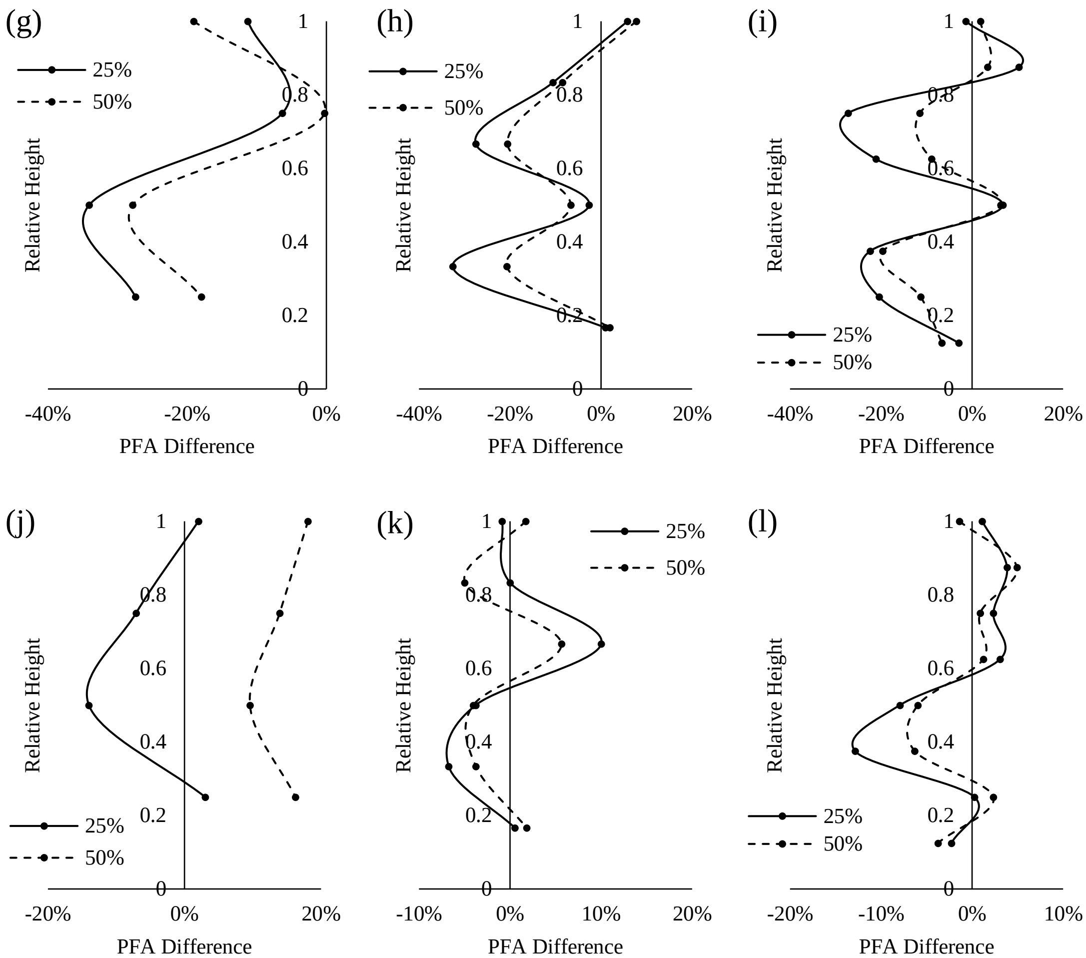

Figure 3.16 continued

3.9 Discussion

By observing the peak floor accelerations presented in Sections 3.4 and 3.6, it can be seen that the values vary for each earthquake record. As expected, the magnitude of the PFAs are consistent with the order of magnitude of the peak ground accelerations (PGAs). However, in real life, damage is not related directly to PGAs. For example, the Mexico earthquake had a PGA of 0.05g while USGS estimated its intensity to be VIII on the Mercalli scale (USGS, M 7.1 - 1km E of Ayutla, Mexico, 2019). On the other hand, Chile earthquake had a PGA of 0.95g with an intensity of VII (USGS, M 6.9 - 40km W of Valparaiso, Chile, 2019).

Two factors that contribute to damage, other than the earthquake magnitude, are frequency content and duration. For example, the Mexico earthquake (260 seconds) is considerably longer than Chile earthquake (70 seconds). Furthermore, because of differences in geology at the respective sites, the Mexico and Chile earthquakes had a different frequency content. Neither of these factors were explicitly accounted for in this particular study.

3.9.1 Hypotheses

In this study three hypotheses were investigated:

3.9.1.1 "Peak floor accelerations profile is a function of the structure"

It can be inferred from Figures 3.5, 3.6, 3.9, 3.10, 3.12 3.13 and 3.13 that PFAs are more affected by the earthquake record than the structure itself. This can be seen by observing the change is PFA when stiffness was manipulated for uniform to non-uniform stiffness models with various damage states.

Although PFA results for the same earthquake record were not perfectly correlated, they were still found to follow a similar pattern along the height of the building.

Compared to the ground motion record, the structural stiffness was found to have less of an effect on the PFA. This conclusion was reached by comparing PFA profiles when damage was increased as the profile is qualitatively close to the undamaged one. However, this is not as vivid as is the correlation in the profile for the difference in the PFA to be discussed next.

Damage location is also not identified through comparison of the PFA profiles. This can be seen when comparing Figures 3.5 with 3.6 where damage location was varied between the first and third floor.

3.9.1.2 "The difference in peak floor accelerations reflects the damage induced"

Figures 3.15 and 3.16 illustrate the difference in PFA for each floor corresponding to the damage states relative to the undamaged model. It can be seen that the way the values change follows the ground motion record for most cases. This is clear for both uniform and non-uniform stiffness models.

It can also be observed from the above-mentioned figures that the PFA follows the same profile throughout the height of the building. For example, the same trend of PFAs for the four-story building is found in the first four levels of the six and eight story buildings. Nevertheless, the relation that governs the change in PFA, whether an increase or decrease, should still to be investigated as it appears to be unique for each record and structure. This agrees with the work of Taghavi et al. (2006), although they used a response spectrum approach. In their study, they showed the importance of considering the correlation between modal responses and ground motion. This was done using the PSD of the record to generate correlation coefficients (Taghavi-Ardakan & Miranda, 2006).

Again, the location of damage was not clearly reflected in the change in the PFA profiles as shown in Figures 3.7 and 3.8 when the damage location was switched from the first floor to the third floor respectively.

3.9.1.3 "Dispersion of the peak floor accelerations increases as the damage is increased"

The variance was calculated for absolute PFA values along the height of the buildings for each record and then plotted vs damage percentage as shown in Figures 3.7, 3.8, 3.11 and 3.14. For some earthquake records the variance decreased when the damage was 25%, but then it increased again. Despite this trend being more pronounced in uniform stiffens structures, some earthquake records responses show different results. This can be related to the frequency content of the ground motion record as it can be exciting specific modes of the structure. Further work should be conducted in this area.

3.9.2 Vulnerability of Structures and Fragility Curves

Vulnerability of buildings after earthquakes is usually estimated by performing a general survey of the area following the earthquake and, in some cases, conducting more in-depth inspections to make sure the structures are usable and there is no risk to the building occupants. One of the popular procedures that is followed for this work is FEMA P-154 (Applied Technology Council, 2015). It relies on a sidewalk inspection to fill in a form in which all of the parameters are used to compute a final score. The score is then compared against the threshold set for vulnerable structures. Depending upon the score, the structure may require a more in-depth inspection or a detailed analysis before it is approved for occupancy (Applied Technology Council, 2015)

Another way to visualize vulnerability is the damage probability matrix (DPM) which was first introduced by Whitman et al. (1973). Using data from previous signature earthquakes and a scale of damage states for similar buildings, a probability matrix was established (Ahmad, Khan, & Pilakoutas, 2015). As is the case with empirical solutions, the larger the data used, the more accurate the matrix will be.

Later, the DPM was further improved and utilized to generate fragility curves, which reflect the probability of exceeding a certain damage state with respect to response or ground motion parameters. Such parameters can be peak ground acceleration (PGA) or story drift.

An example of using PGA for fragility curves is given by Ahmad et al. (2015) who studied non-engineered buildings in a region in Pakistan after the Kashmir earthquake (2005). The damage was studied with PGA and fragility curves were created for damage vs PGA (Ahmad, Khan, & Pilakoutas, 2015).

Using story drift to construct fragility curves can be more reliable than when using other parameters since it has a direct relationship to damage through the force-capacity relationship. Many researchers have invested effort in evaluating the drift capacity of different types of construction. Erduran et al. (2004) performed non-linear finite element analysis for a column experiment conducted by Azizinamini et al. (1988) (Azizinamini, Johal, Hanson, Musser, & Corley, 1988) and was able to generate the same results to validate the model. The work then was expanded to study a number of factors that contribute to a column ductility and it was found that damage is directly effected by drift and yield drift. It was also found that drift is a function of column properties such as slenderness and the yield strength of longitudinal bars. While shear reinforcement ratio didn't effect the yield drift, it was found to contribute, in a direct relationship, to the ultimate drift ratio. On the other hand, the axial load was not determined to govern yield drift. However, increased axial loading lowered ultimate ductility as per the conducted analysis (Erduran & Yakut, 2004).

In applying this knowledge, most typical (non-code-regulated) buildings follow a typical column-spacing and story height; thus, loading for the same usage and slenderness can be estimated. In addition, they share typical column reinforcement in terms of material strength and quantities leading to the potential of estimating a critical drift ratio that can be used as a threshold for a certain damage state. Although thresholds are established by FEMA 356 (American Society of Civil Engineers, 2000), they can be refined for each region to reflect common structural characteristics. In Chapter 4, a variety of techniques used to measure drift are discussed.

Chapter 4

DISPLACEMENT-DAMAGE RELATIONSHIP

Going back to the fundamentals of mechanics of materials, Hook's law relates force directly to displacement through stiffness; for linear elastic behavior. With the force known for a given structure, damage can be estimated. In other words, damage detection in structures can be achieved by solely monitoring displacement as it relates directly to forces, and thus, damage levels. FEMA-445 (Applied Technology Council, 2006) considers inter-story drift as a parameter which can be used efficiently as an indicator of how much damage a structure will suffer. However, predicting a drift value for a real structure subjected to an earthquake is quite complicated and depends on several factors such as stiffness, damping ratio, material modeling, mass distribution and, most importantly, ground motion. From a modeling perspective, to evaluate displacement, e.g. for performance-based design, the modeled structure has to be subjected to a number of ground motion records and the results plotted as a random distribution where the median value is used (Applied Technology Council, 2006). In real life applications, measuring the drift parameter for a particular seismic event is still considered a cumbersome process, it has to be done during the earthquake event in which it is difficult to keep sensors working and measurements accurate. Therefore, a variety of approaches were developed to estimate peak seismic displacement/drift such as double integration of the acceleration signal, using residual drift to estimate peak drift, and optical methods including laser crosshair and digital image correlation.

4.1 Double Integration of Acceleration Records

Double integration of a recorded acceleration signal is a commonly used method to determine inter-story drift. It has been found that this approach is relatively accurate (5% error) in cases of linear behavior; however, where nonlinearity exists, the error can reach up to 12% for peak values. It also requires an extensive instrumentation for the buildings where accelerometers should be placed on every floor; otherwise, using interpolation for data from missing floors will increase the error in the estimated drift values. (Skolnik & Wallace, 2010)

4.2 Residual Drift

Residual drift is the permanent horizontal displacement that exists at the end of an earthquake. It can be effected by ground motion intensity, structural behavior, and site characteristics (Dai, Wang, BoweiLi, & H.P.Hong, 2017). The peak displacement can then be predicted using either the residual displacement ratio presented by Ruiz-Garcia et al. work (Ruiz-García & Miranda, 2006) or the one presented by Hatzigeorgiou et al. (Hatzigeorgiou, Papagiannopoulos, & Beskos, 2011) where empirical equations are generated using regression based on the results of parametric non-linear analysis for SDOF structure subjected to a large number of earthquake records.

Use of residual drift has a great potential in conjunction with the advances in the aerial and satellite imaging. Large areas can be inspected quickly by comparing images before and after the seismic event. While it is promising, it is still a non-traditional approach as it does not follow the same direct elastic force-displacement relationship.

4.3 Laser Crosshair Method

Bennett et al. (1996) presented a method of using laser crosshair techniques to accurately measure displacement and rotation among all stories to estimate inter-story drift. Although the measurements are highly accurate, it requires that a laser beam be generated, a set of mirrors, beam splitter and four photodetectors for each floor (Bennett & Batroney, 1996). In 1998, Chen et al. followed up on this work and carried out experimental work to validate the proposed technique resulting in accuracy of 10 microns for lateral displacement and a 0.02 degrees of rotation between two consecutive floors, which should be enough for the most research applications (Chen, Bennett, Feng, Wang, & Huang, 1998). This setup can be practical for experimental purposes, but it is not the case if it will be used to monitor actual buildings due to its complexity and high cost to maintain it as a health monitoring system.

4.4 Digital Image Correlation (DIC)

Digital image correlation is currently used for different scientific and daily life applications. As it advances, and its accuracy increases, it becomes promising for different fields such as structural experiments and structural health monitoring.

Early methods included fringe projection over monitored object and then analyzing images taken by a digital camera for the projection. Changes in fringe patterns are then transformed into displacement using a specific algorithm. The advantage of this method is that it can provide out of plane as well as in plane displacement, so a 3D displacement can be generated using this method (Quan, Tay, & Huang, 2004). The need for a projection device and a controlled environment to perform the process makes it difficult to be used in real life health monitoring applications.

With the boom in image processing applications, a more compact, simple, and efficient way of sensing has emerged. A high-resolution camera with a well-crafted algorithm can substitute a large number of strain, tilt, and acceleration sensors in a single experiment. Mirzazadeh et al. (2018) have used DIC to measure deformations in RC beams and found that it can be effective in measuring deflections and crack widths. The results for displacement were compared to potentiometer readings and the accuracy was found to be comparable to the potentiometers; however, it depends on calibrating the measurement for a number of identified sources of error including: temperature variation and the coefficients of thermal expansion of the camera and the setup, lighting conditions and variability during the experiment, and movement of the target in the out-of-plane direction (Mirzazadeh & Green, 2018).

Sieffert et al. (2016) used this technique in a test involving a shake table for a prototype of a wooden frame with walls filled with stone and earth where its strength and capability to withstand seismic loading was checked. This type of construction was inspired from Haitian culture and can provide a great alternative to reinforced concrete systems in poor remote areas. The structure (see Figure 4-1) was subjected to a number of ground motions while being monitored by a high-speed camera.

Figure 4.1 Monitored structure using DIC (reprinted from (Sieffert, et al., 2016))

A parallel instrumentation system was also used to verify results obtained by DIC. The maximum difference obtained between the two methods was 5%, which indicates a promising future for the DIC technique used in structural experiments. Figures 4.1 and 4.2 show the monitored structure and displacement results obtained by DIC respectively. By tracking multiple points, damage and de-bonding were identified easily in this study. This is a great example of the flexibility of this technique in selecting multiple points of interest without requiring additional instrumentation, even after the test had been performed (Sieffert, et al., 2016).

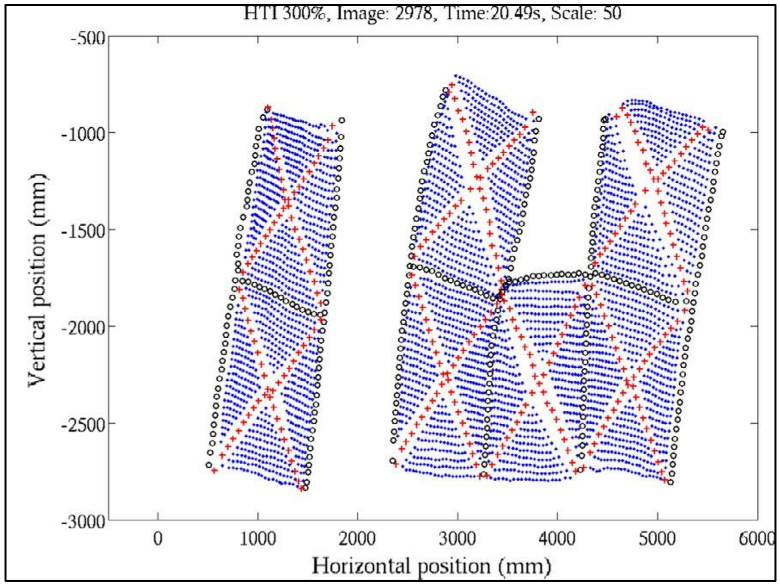

Figure 4.2 Displacement obtained by DIC (reprinted from (Sieffert, et al., 2016))

While using high-quality components can improve the accuracy of the measurements, the DIC technique can be applied using low-cost components and provide reasonable results. A paper was published by Wang et al. (2018) in which they were successful in capturing multiple simulated ground motion records using an Apple IPhone6 camera and a target on a shaking table. The results were used to construct a power spectrum density (PSD) diagram. Meanwhile, a parallel measurement system using a laser displacement sensor was used to verify the DIC results. Although the error in peak location in the PSD reached 10% in some cases, a good match was observed with correlation coefficients between the two systems, for both the displacement and the PSD, results exceeding 0.998 in some cases and 0.999 in most of them (Wang, Ri, Liu, & Zhao, 2018).

The majority of attempts to measure displacements in structures using DIC that are published in literature were performed in the lab. Even with the few experiments that were carried out in the field, they shared the same setup of the camera monitoring the structure from outside. For a structural health monitoring system, it is favorable to be compact and attached to the structure in a permanent setup because having a vantage point for each structure is a challenge on its own. For this reason, some people worked on the idea of measuring differential displacement through a series of low-cost cameras and targets over the height of the building. This is exactly what was proposed by Park et al. (2010) and was tested in the lab by attaching a series of webcams and targets on a cantilever steel column and subjected to two load cases. The results were promising with a percentage of error less than 1% for the displacement with reference to laser displacement sensor measurements. However, results were off by 74% when the rotational angle was used to estimate the displacement (Park, Lee, Jung, & Myung, 2010). This implies that such a technique can be highly accurate in measuring displacement directly even when low-cost equipment is used.

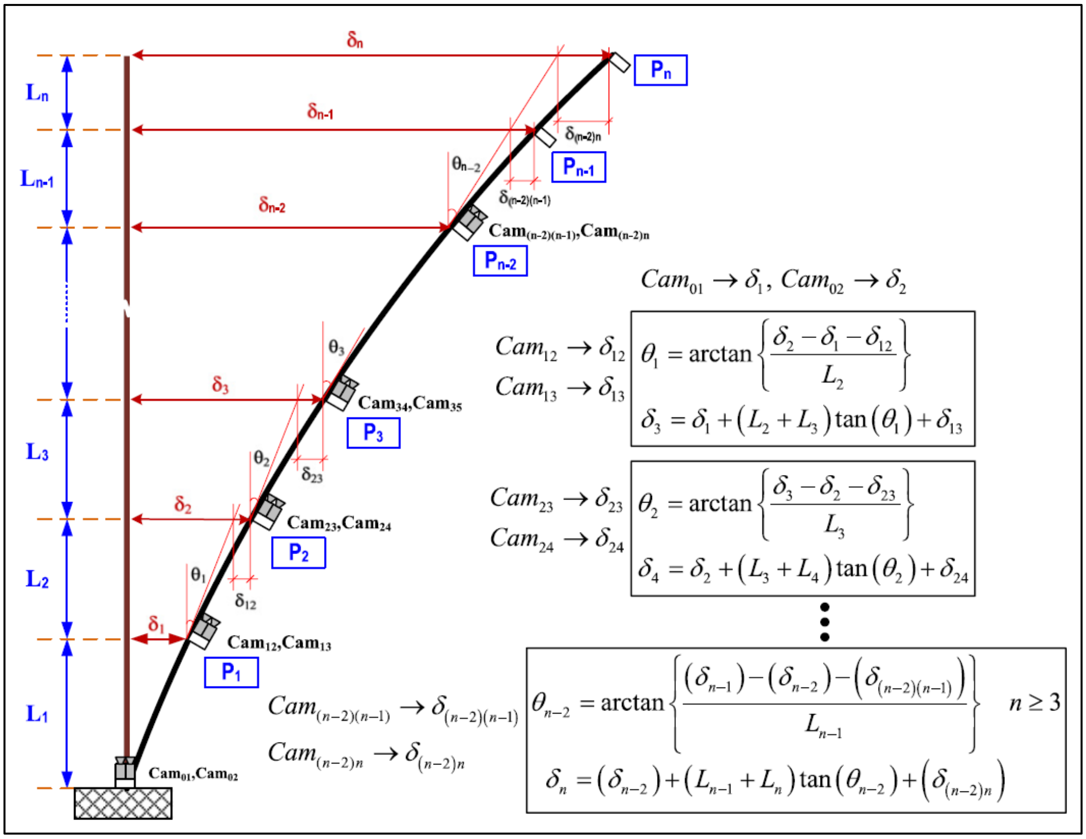

Figure 4.3 Proposed DIC displacement measurement system (reprinted from (Lee, Ho, Shinozuka, & Lee, 2012))

Later, to verify the proposed method, Lee et al. (2012) tested a full-scale four-story steel frame. It was excited using either sinusoidal or random vibration and the displacements were recorded. Although results were verified using a single point measurement system (from a vantage point), the matching of the results within a 2% maximum error is an indication of the great potential of the system (Lee, Ho, Shinozuka, & Lee, 2012).

Chapter 5

LIMITATIONS

The techniques presented in this study present the possibility of being useful for post-earthquake damage detection. However, to achieve such a goal, a number of limitations must first be overcome. These limitations will now be described.

5.1 Analytical Approach Limitations

When computer models are used to estimate real world response, all simplifications, assumptions, and shortcuts involved in the modeling process will effect the accuracy of the results. A good example of such factors is the presence and type of partitions. Devin et al. (2015) studied an actual building and found that partitions and cladding increase the frequency of the floor up to 30% for some floors and this increase was a function not only of the type of partition, but also their distribution over the floor (Devin, Fanning, & Pavic, 2015). Another factor that comes into play is soil-structure interaction. Its effect can be observed on recorded accelerations in buildings. Anajafi et al. (2018) assumed that buildings mostly behave linearly-elastic based on the data they studied as they noticed that peak acceleration recorded at the base of the monitored structures is significantly lower than the peak ground acceleration in that region (Anajafi & Medina, 2018). Finally, using a linear elastic approach inhibited the ability to simulate stiffness degradation with time, which can be critical if we consider the duration of the seismic event.

5.2 Hardware Limitations

In addition to the approach limitations, hardware development to meet the need of innovative ideas is another challenge. The following discusses some of the issues that rapid structural inspection might run in to.

5.2.1 Shock Gauges

By using shock gauges, the time dimension is absent, and if the maximum acceleration takes place when the structure is in an undamaged state, and then the building is damaged during the earthquake it may fail to capture the damaged state response. Unless the acceleration values of the damaged state are higher, the new condition won't be reflected on the gauges.

5.2.2 Simple Low-Cost Accelerometers

It is found to be complicated to specify floor acceleration thresholds to wake up the low-cost sensors. In addition, the ability to link the damage to peak floor accelerations has not yet been established. By contrast, displacement and drift measurements represent a more promising approach.

5.2.3 DIC Technique

The DIC technique has great promise in structural damage detection. However, as mentioned in this study, a number of challenges still need to be overcome. First, the temperature calibration and differences in thermal coefficients add to the complexity of the system. Then, variation in light conditions can affect the measurements. Finding a location in the building where light conditions are controlled at all times may not be a simple exercise. Finally, large data size storage, transmitting, and processing poses challenges also exist.

In addition to the afore mentioned limitations, when operating a network of sensors, especially over a wireless network, the following issues are expected to affect the process.

5.2.4 Synchronization

Li et al. (2016), in an effort to develop a new method to help better synchronize sensors data in a wireless network, mentioned several sources of synchronization errors such as slight random variabilities in the quality of electronic components that can affect the sampling rate and thus, the synchronization among the network. Having some sensors exposed to heat sources (e.g. sun light) can also slightly shift the sensor clock by effecting quartz crystal properties inside. In addition, the time needed to awaken all of the devices in the network from their sleep mode and get them synchronized before capturing data can take up to 30s, which sometimes is sufficient, to miss the event (Li, Mechitov, Kim, & Jr., 2016).

5.2.5 Large Data Acquisition

Beside reliability concerns, having sensors acquire data over an extended period of time can lead to other types of errors that should be accounted for. Such errors can arise from the increase of temperature when the electronic boards are left running for a long time. The DIC technique mentioned in Section 4.4 is susceptible to this type of errors and was studied by Ma et al. (2012). They determined the error to be as large as 230με strain, which in some cases (such as crack width measurement) can be significant where the resolution is vital. This error is mainly due to the uneven expansion of the sensor geometry. However, with proper calibration and correction that accounts for the components' temperature, it can be overcome (Ma, Pang, & Ma, 2012).

5.2.6 Realtime Processing

Realtime data processing is the optimum system when it comes to SHMSs. The realtime systems should be capable of providing the public the basic info about the post-earthquake safety of the structure. However, with the current technology, realtime processing is requires hardware with high-end specs and large storage capacities to store the resulting data.

In the future, new solutions will be developed. If reliable connections that enables the use of cloud processing during the earthquake can be developed, realtime or near realtime processing may become a reality.

Chapter 6

CONCLUSIONS AND FUTURE WORK

6.1 Conclusions

In the first part of this thesis, peak floor accelerations were studied for multiple damage states of hypothetical buildings through linear time-history analysis. PFA profiles were found to be more sensitive to the earthquake record than to the damage state or to the stiffness distribution along the building. However, all the afore mentioned factors contribute to the PFA profile. The difference in PFA values with damage to the PFA values without damaged was determined to follow the ground motion record with a similar fashion for various building heights. The relationship of variance of PFA with damage requires more investigation and should consider the frequency content of the ground motion in combination with the dynamic properties of the structure.

Using displacements appears to be more promising when it comes to rapid structural inspection and damage detection. Displacement can be measured by a variety of methods including, but not limited to, double integration of acceleration records, residual drift, laser methods, and digital image correlation. With recent technological advances, it has become possible to measure the displacement directly using DIC techniques, rather than the indirect methods such as double integration of the acceleration signal. DIC techniques present the potential to provide a cost-effective SHMS solution that extends even for typical or non-essential structures.

6.2 Future Work

Future work includes non-linear time-history analysis that considers the duration as well as stiffness degradation of the structure during the earthquake. Future work should also investigate other structural systems such bearing walls system, building frame systems, or dual systems. Several iterations can be carried out for time-history analysis using ground motion records from the same site location. The results can verify the effect of the site-specific characteristics on the PFA profile.

To transition the results of this study into practice, instrumentation of actual buildings should be conducted. This instrumentation should include placing accelerometers on all floor levels including base level. In addition, having a field sensor outside the building to measure the PGA in-situ so that it can be compared to the measured value at the base will be useful to quantify the effect of soil-structure interaction on base excitation. Performing analyses based on the measured data will yield more reliable conclusions. Location of the structure from the epicenter, or the recording station, should also be considered to further expand this work.

In order to achieve an area-wide SHMS, methods have to be developed to approximate values for non-instrumented buildings using data obtained from instrumented ones. Such methods should consider the geographic location of the structures, partitions and other non-structural components and their effect on the dynamic behavior of the structure, as well as soil-structure interactions.

REFERENCES

Ahmad, S., Khan, S. A., & Pilakoutas, K. (2015). Empirical vulnerability assessment of the non-engineered reinforced concrete structures using the Kashmir earthquake damage data. *Bull Earthquake Eng Bulletin of Earthquake Engineering : Official Publication of the European Association for Earthquake Engineering, 13*, 2611-2628.

American Society of Civil Engineers. (2000). *FEMA 356 Prestandard And Commentary for The Seismic Rehabilitation Of Buildings.* Washington, D.C.: Federal Emergency Management Agency.

American Society of Civil Engineers Staff (ASCE). (2013). *Minimum Design Loads for Buildings and Other Structures.* Reston: American Society of Civil Engineers.

Anajafi, H., & Medina, R. (2018). Evaluation of ASCE 7 equations for designing acceleration-sensitive nonstructural components. *Eleventh U.S. National Conference on Earthquake Engineering.* Los Angeles, California.

Applied Technology Council. (2006). *FEMA-445 Next-Generation Performance-Based Seismic Design Guidelines: Program Plan for New and Existing Buildings.* Washington, D.C.: Federal Emergency Management Agency.

Applied Technology Council. (2015). *FEMA P-154 Rapid Visual Screening of Buildings for Potential Seismic Hazards: A Handbook.* Washington, D.C.: Federal Emergency Management Agency.

Azizinamini, A., Johal, L. S., Hanson, N. W., Musser, D. W., & Corley, W. G. (1988). *Effects of transverse reinforcement on seismic performance of columns: A partial parametric investigation.* Washington, D.C.: National Science Foundation.

Bennett, K. D., & Batroney, C. B. (1996). Laser crosshair projection technique for interstory drift measurement. *Proceedings- SPIE The International Society For Optical Engineering*, 302-310.

Chen, W., Bennett, K. D., Feng, J., Wang, Y.-P., & Huang, S. (1998). Laser technique for measuring three-dimensional interstory drift. *Proceedings of SPIE*, (pp. 305-310). Beijing, China.

Dai, K., Wang, J., BoweiLi, & H.P.Hong. (2017). Use of residual drift for post-earthquake damage assessment of RC buildings. *Engineering Structures 147*, 242-255.

Devin, A., Fanning, P. J., & Pavic, A. (2015). Modelling effect of non-structural partitions on floor modal properties. *Engineering Structures 91*, 58–69.

Erduran, E., & Yakut, A. (2004). Drift based damage functions for reinforced concrete columns. *Computers and Structures*, 121–130.

Hatzigeorgiou, G. D., Papagiannopoulos, G. A., & Beskos, D. E. (2011). Evaluation of maximum seismic displacements of SDOF systems from their residual deformation. *Engineering Structures 33*, 3422–3431.

Huang, M. J., & Shakal, A. (2001). in Proceedings. *Invited Workshop on Strong-motion Instrumentation of Buildings* (pp. 15-19). Emeryville, Ca: COSMOS.

Lee, J.-H., Ho, H.-N., Shinozuka, M., & Lee, J.-J. (2012). An advanced vision-based system for real-time displacement measurement of high-rise buildings. *Smart Materials and Structures, 21*, 125019 (10pp).

Li, J., Mechitov, K. A., Kim, R. E., & Jr., B. F. (2016). Efficient time synchronization for structural health monitoring using wireless smart sensor networks. *Structural Control and Health Monitoring*, *23*, 470-486.

Ma, S., Pang, J., & Ma, Q. (2012). The systematic error in digital image correlation induced by self-heating of a digital camera. *Measurement Science and Technology*, *23*, 025403 (7pp).

Marshall, J. D., Jaiswal, K., Gould, N., Turner, F., Lizundia, B., & Barnes, J. C. (2013). Post-earthquake building safety inspection: Lessons from the

Canterbury, New Zealand, earthquakes. *Earthquake Spectra*, *29*(3), 1091-1107.

Mirzazadeh, M. M., & Green, M. F. (2018). Fiber optic sensors and digital image correlation for measuring deformations in reinforced concrete beams. *Journal of Bridge Engineering*, *ASCE*, 04017144 1-5.

Mita, A., & Takahira, S. (2002). In Proceedings. *Proceedings of the International Conference on Advances in Building Technology* (pp. 521-528). Hong Kong, China: Elsevier.

Park, J.-W., Lee, J.-J., Jung, H.-J., & Myung, H. (2010). Vision-based displacement measurement method for high-rise building structures using partitioning approach. *NDT & E International, 43*, 642-647.

Pozzi, M., & Kiureghian, A. D. (2015). Response spectrum analysis for floor acceleration. *Earthquake Engineering & Structural Dynamics 44*, 2111– 2127.

Quan, C., Tay, C. J., & Huang, Y. (2004). 3-D deformation measurement using fringe projection and digital image correlation. *International Journal for Light and Electron Optics, 115*(4), 164-168.

Ruiz-García, J., & Miranda, E. (2006). Residual displacement ratios for assessment of existing structures. *EQE Earthquake Engineering & Structural Dynamics*, 315-336.

Shan, J., Yang, H. T., Shi, W., Bridges, D., & Hansma, P. K. (2013). Structural damage diagnosis using interstory drift–based acceleration feedback with test validation. *Journal of Engineering Mechanics*, 1185-1196.

Sieffert, Y., Vieux-Champagne, F., Grange, S., Garnier, P., Duccini, J. C., & Daudeville, L. (2016). Full-field measurement with a digital image correlation analysis of a shake table test on a timber-framed structure filled with stones and earth. *Engineering Structures*(123), 451–472.

Skolnik, D. A., & Wallace, J. W. (2010). Critical assessment of interstory drift measurements. *Journal of Structural Engineering Vol. 136*, 1574-1584.

Taghavi-Ardakan, S., & Miranda, E. (2006, June). *Probabilistic seismic assessment of floor acceleration demands in multi-story buildings.* Stanford CA: John A. Blume Earthquake Engineering Center .

USGS. (2019, Jan 21). *Latest Eqarthquakes*. Retrieved from USGS Website: https://earthquake.usgs.gov/

USGS. (2019, 6 6). *M 6.9 - 40km W of Valparaiso, Chile*. Retrieved from USGS Earthquake Hazards Program: https://earthquake.usgs.gov/earthquakes/eventpage/us10008kce/executive

USGS. (2019, 6 6). *M 7.1 - 1km E of Ayutla, Mexico*. Retrieved from USGS Earthquake Hazards Program: https://earthquake.usgs.gov/earthquakes/eventpage/us2000ar20/executive#executive

Wang, N., Ri, K., Liu, H., & Zhao, X. (2018). Structural displacement monitoring using smartphone camera and digital image correlation. *IEEE Sensors Journal*, 4664-4672.

Appendix A

MODIFIED CQC METHOD – WORK FROM LITERATURE

A.1 Taghavi et al. Work

The following summarizes effort of Taghavi et al. for to determine PFA using response spectrum and modified CQC combination method:

$$\ddot{u}_k^t(x,t) \cong \ddot{u}_g(t) + \sum_{i=1}^{n} \Gamma_i \phi_{ik}(x) \ddot{D}_i(t)$$

$$PFA_k = \left[\left(\frac{P_k^T}{P_g}\right)^2 PGA^2 + \sum_{i=1}^{N}\sum_{j=1}^{N} \Gamma_i \Gamma_j \phi_{ik} \phi_{jk} \left(\frac{P_k^T}{P_i}\right)\left(\frac{P_k^T}{P_j}\right) S_{aR,i} S_{aR,j} \rho_{\ddot{D}_i(t),\ddot{D}_j(t)} \right.$$
$$\left. + 2 \times PGA \times \sum_{j=1}^{N} \Gamma_i \phi_{ik} \left(\frac{P_k^T}{P_i}\right)\left(\frac{P_k^T}{P_g}\right) S_{aR,i} \rho_{\ddot{u}_g(t),\ddot{D}_i(t)} \right]^{1/2}$$

$$PFA_k = \max\left(\ddot{u}_k^T(t)\right) = P_k^T \sigma_{\max\left(\ddot{u}_k^T(t)\right)}$$

$$PGA = \max\left(\ddot{u}_g(t)\right) = P_g \sigma_{\max\left(\ddot{u}_g(t)\right)}$$

$$S_{aR,i} = \max\left(\ddot{D}_i(t)\right) = P_i \sigma_{\max\left(\ddot{D}_i(t)\right)}$$

$$E\left[\ddot{D}_i(t)\ddot{D}_j(t)\right] = Re\left[\int_0^{\infty} \omega^4 G_F(\omega) H_i(\omega) \mathrm{H}_j{}^*(\omega) d\omega\right] = \lambda_{4,ij}$$

$$\rho_{ij} = \frac{\lambda_{4,ij}}{\sqrt{\lambda_{4,ii}\lambda_{4,jj}}}$$

$$\rho_{ig} = \frac{\omega_i{}^2 \lambda_{2,ij} - \lambda_{4,ij}}{\sqrt{E\left[\ddot{u}_g(t)^2\right]\lambda_{4,ii}}}$$

Where,

P_k, P_g, P_i, P_j	: Peak factors
PFA_k	: Peak floor acceleration at level k

PGA	: Peak ground acceleration
Γ_i	: Modal participation factor for mode i
ϕ_{ik}	: Modal shape matrix value at floor k for mode i
$S_{aR,i}$	: Modal relative acceleration for mode i
$\rho_{\ddot{D}_i(t),\ddot{D}_j(t)}$	: Correlation coefficient for relative modal acceleration
$\rho_{\ddot{u}_g(t),\ddot{D}_i(t)}$	: Correlation coefficient between ground acceleration and relative modal acceleration for mode i

For the peak factors, Taghavi et al. determined that if the period of the mode is less than one second, then they can be considered unity without considerable error. For longer periods (lower modes), they used the results of the model they developed (Flexural beam and shear beam connected with axially-rigid links), was not mentioned here, subjected to a number of earthquake records. Assuming uniform stiffness, and 5% damping ratio the following relations were provided to estimate the peak factors (Taghavi-Ardakan & Miranda, 2006):

$$PF_{ij}^{k} = \left(\frac{P_k^T}{P_i}\right)\left(\frac{P_k^T}{P_j}\right)$$

$$PF_{00} = 1 - 0.45\sin\left(\frac{\pi x}{1.7}\right)$$

$$PF_{0\mathrm{j}} = \frac{PF_{\mathrm{ij}}}{\mathrm{SC}_j}$$

$$PF_{\mathrm{ij}} = PF_{00} \times \mathrm{SC}_i \times \mathrm{SC}_j$$

$$\mathrm{SC}_i = 1 + 0.272i - 0.112i^2 + 0.0111i^3$$

Where,

PF_{00}	: Peak factor ratio for ground acceleration
x	: Relative elevation, x=0 at the base

PF_{ij}	: Peak factor ratio for modes i and j
k	: Floor level considered

A.2 Moschen et al. Work

$$\max(|\ddot{u}\text{^}((tot)\ )\ (t)|) = \mathrm{PFA} \approx \left[\sum_{i=1}^{n}\sum_{j=1}^{n}\phi_i\phi_j\Gamma_i\Gamma_j S_{a,i}^{(rel)} S_{a,j}^{(rel)} \frac{p_i p_j}{{p_g}^2}\rho_{ij} + 2PGA \times \sum_{j=1}^{n}\phi_i\Gamma_i S_{a,j}^{(rel)} \frac{p_i}{p_g}\rho_{ig} + \mathrm{e}PGA^2\right]^{1/2}$$

$$S_a^{(rel)}(T) = S_a^{(abs)}(T) - f(T)$$

$$\rho_{ij}^{*} = \frac{p_i p_j}{{p_g}^2}\rho_{ij}$$

$$\rho_{ij}^{*} \approx \beta_0 + \sum_{k=1}^{2}\left[\beta_{k,1}\tanh\left(\left(\frac{1}{\bar{T}_i} + \beta_{k,2}\right)\beta_{k,3} + \sum_{l=0}^{4}\left(\frac{\gamma_{k,1}}{|\bar{T}_j{}^{l}|}\right)\right)\right]$$

$$\begin{pmatrix}\bar{T}_i \\ \bar{T}_j\end{pmatrix} = \begin{bmatrix}\cos(\pi/4) & \sin(\pi/4) \\ -\sin(\pi/4) & \cos(\pi/4)\end{bmatrix}\begin{pmatrix}T_i \\ T_j\end{pmatrix}$$

$$\rho_{ig}^{*} = \frac{p_{ig}}{p_g}\rho_{ig}$$

$$\rho_{ig}^{*} = \sum_{k=1}^{2}\delta_{k,1}e^{\delta_{k,2}/T_i}$$

Where,

p_i, p_j, p_g	: Peak factors
PFA	: Peak floor acceleration
PGA	: Peak ground acceleration
Γ_i	: Modal participation factor for mode i
ϕ_i	: Modal shape matrix value at floor k for mode i
$S_{a,i}^{(rel)}$	: Modal relative acceleration for mode i
ρ_{ij}	: Correlation coefficient for relative modal acceleration

ρ_{ig} : Correlation coefficient between ground acceleration and relative modal acceleration for mode i

Appendix B

TABLES

Table B.1 Four-story building PFA – First story damage

Level	El-Centro EQ			Mexico EQ			Chile EQ			New Zealand EQ		
	UD	25%	50%	UD	25%	50%	UD	25%	50%	UD	25%	50%
#	in/s^2	in/s^2	in/s^2	in/s^2	in/s^2	in/s^2	in/s^2	in/s^2	in/s^2	in/s^2	in/s^2	in/s^2
4	344	354	317	41.9	46.8	49.8	399	354	323	343	350	405
3	313	320	313	34	44.1	38	364	341	363	366	340	417
2	283	280	310	30.4	38.2	32.6	575	379	415	407	350	446
1	214	211	219	17.7	28.2	25	529	384	434	363	374	422
0	0	0	0	0	0	0	0	0	0	0	0	0

Table B.2 Four-story building variance calculation $(a\text{-}a_{avg})^2$ – First story damage

Level	El-Centro EQ			Mexico EQ			Chile EQ			New Zealand EQ		
#	UD	25%	50%	UD	25%	50%	UD	25%	50%	UD	25%	50%
4	3080.3	3937.6	742.6	118.8	55.9	180.9	4590.1	110.3	3690.6	715.6	12.3	306.3
3	600.3	826.6	540.6	9.0	22.8	2.7	10557.6	552.3	430.6	14.1	182.3	30.3
2	30.3	126.6	410.1	0.4	1.3	14.1	11718.1	210.3	976.6	1387.6	12.3	552.3
1	5550.3	6440.1	5005.6	176.9	123.8	128.8	3875.1	380.3	2525.1	45.6	420.3	0.3
0	0.0	0.0	0.0	0.0	0.0	0.0	0.0	0.0	0.0	0.0	0.0	0.0
Var	3087.0	3776.9	2232.9	101.7	67.9	108.8	10246.9	417.7	2540.9	720.9	209.0	296.3

Table B.3 Four-story building PFA – Third story damage

Level	El-Centro EQ			Mexico EQ			Chile EQ			New Zealand EQ		
	UD	25%	50%	UD	25%	50%	UD	25%	50%	UD	25%	50%
#	in/s^2	in/s^2	in/s^2	in/s^2	in/s^2	in/s^2	in/s^2	in/s^2	in/s^2	in/s^2	in/s^2	in/s^2
4	344	351	366	41.9	45.1	48.7	399	321	339	343	390	370
3	313	327	317	34	38.4	40.4	364	360	360	366	406	423
2	283	278	278	30.4	41.4	39.1	575	418	471	407	428	445
1	214	219	230	17.7	24	22.9	529	555	517	363	442	425
0	0	0	0	0	0	0	0	0	0	0	0	0

Table B.4 Four-story building variance calculation $(a-a_{avg})^2$ – Third story damage

Level	El-Centro EQ			Mexico EQ			Chile EQ			New Zealand EQ		
#	UD	25%	50%	UD	25%	50%	UD	25%	50%	UD	25%	50%
4	3080.3	3277.6	4658.1	118.8	62.0	119.4	4590	8556.3	6847.6	715.6	702.3	2093.1
3	600.3	1105.6	370.6	9.0	1.4	6.9	10558	2862.3	3813.1	14.1	110.3	52.6
2	30.3	248.1	390.1	0.4	17.4	1.8	11718	20.3	2425.6	1387.6	132.3	855.6
1	5550.3	5587.6	4590.1	176.9	174.9	221.3	3875.1	20022	9072.6	45.6	650.3	85.6
0	0.0	0.0	0.0	0.0	0.0	0.0	0.0	0.0	0.0	0.0	0.0	0.0
Var	3087.0	3406.3	3336.3	101.7	85.2	116.4	10247	10487	7386.3	720.9	531.7	1028.9

Table B.5 Six-story building PFA – Uniform stiffness

Level	El-Centro EQ			Mexico EQ			Chile EQ			New Zealand EQ		
	UD	25%	50%	UD	25%	50%	UD	25%	50%	UD	25%	50%
#	in/s^2	in/s^2	in/s^2	in/s^2	in/s^2	in/s^2	in/s^2	in/s^2	in/s^2	in/s^2	in/s^2	in/s^2
6	265	287	281	60.3	63.7	70.4	394	370	391	359	351	350
5	244	244	244	53.1	53.6	66.6	355	350	346	316	348	341
4	221	226	213	48.1	57.1	59.4	411	362	359	347	353	353
3	173	181	189	35.4	57	48.8	305	366	337	356	351	350
2	174	163	156	28.7	53.1	37.2	520	375	461	392	363	371
1	160	158	171	15.6	42.3	30.5	510	399	464	394	383	391
0	0	0	0	0	0	0	0	0	0	0	0	0

Table B.6 Six-story building variance calculation $(a-a_{avg})^2$ – Uniform stiffness

Lev -el	El-Centro EQ			Mexico EQ			Chile EQ			New Zealand EQ		
#	UD	25%	50%	UD	25%	50%	UD	25%	50%	UD	25%	50%
6	3461.4	5954.7	5184.0	404.0	85.3	333.1	476.7	0.1	4.0	2.8	51.4	87.1
5	1431.4	1167.4	1225.0	166.4	0.8	208.8	3700.7	413.4	2209.0	1995.1	103.4	336.1
4	220.0	261.4	16.0	62.4	6.9	52.6	23.4	69.4	1156.0	186.8	26.7	40.1
3	1100.0	831.4	400.0	23.0	6.4	11.2	12284	18.8	3136.0	21.8	51.4	87.1
2	1034.7	2193.4	2809.0	132.3	1.9	223.5	10851	21.8	4624.0	981.8	23.4	136.1
1	2131.4	2686.7	1444.0	605.2	148.0	468.7	8867.4	821.8	5041.0	1111.1	616.7	1002.8
0	0.0	0.0	0.0	0.0	0.0	0.0	0.0	0.0	0.0	0.0	0.0	0.0
Var	1875.8	2619.0	2215.6	278.7	49.9	259.6	7240.6	269.1	3234.0	859.9	174.6	337.9

Table B.7 Eight-story building PFA – Uniform stiffness

Level	El-Centro EQ			Mexico EQ			Chile EQ			New Zealand EQ		
	UD	25%	50%	UD	25%	50%	UD	25%	50%	UD	25%	50%
#	in/s^2	in/s^2	in/s^2	in/s^2	in/s^2	in/s^2	in/s^2	in/s^2	in/s^2	in/s^2	in/s^2	in/s^2
8	259	248	224	77.2	44.1	68.2	433	379	396	364	347	355
7	210	200	187	72.3	42.1	63.7	350	372	365	384	350	361
6	168	166	164	65.3	40.6	58.7	331	364	356	345	351	352
5	180	174	154	58.1	36.9	56	358	346	331	329	351	344
4	206	188	173	49.9	35.1	49.3	438	358	378	335	352	343
3	234	229	216	49.1	36	45.1	382	352	369	336	351	343
2	249	247	236	35.8	30.9	35	470	370	401	392	365	378
1	165	174	187	15.9	21.7	19.3	461	398	432	408	381	406
0	0	0	0	0	0	0	0	0	0	0	0	0

Table B.8 Eight-story building variance calculation $(a-a_{avg})^2$ – Uniform stiffness

Lev-el	El-Centro EQ			Mexico EQ			Chile EQ			New Zealand EQ		
#	UD	25%	50%	UD	25%	50%	UD	25%	50%	UD	25%	50%
8	2512.5	2002.6	984.4	588.1	66.8	353.0	907.5	135.1	306.3	5.6	81.0	27.6
7	1.3	10.6	31.6	374.4	38.1	204.1	2795.8	21.4	182.3	500.6	36.0	0.6
6	1670.8	1387.6	819.4	152.5	21.9	86.3	5166.0	11.4	506.3	276.4	25.0	68.1
5	833.8	855.6	1491.9	26.5	1.0	43.4	2013.8	456.9	2256.3	1064.4	25.0	264.1
4	8.3	232.6	385.1	9.3	0.7	0.0	1233.8	87.9	0.3	708.9	16.0	297.6
3	631.3	663.1	546.4	14.8	0.0	18.6	435.8	236.4	90.3	656.6	25.0	297.6
2	1610.0	1914.1	1881.4	294.1	25.3	207.7	4505.8	6.9	506.3	922.6	81.0	315.1
1	1925.0	855.6	31.6	1372.7	202.4	906.8	3378.5	937.9	2862.3	2150.6	625.0	2093.1
0	0.0	0.0	0.0	0.0	0.0	0.0	0.0	0.0	0.0	0.0	0.0	0.0
Var	1313.3	1131.6	881.7	404.6	50.9	260.0	2919.6	270.6	958.6	898.0	130.6	480.5

Table B.9 Six-story building PFA – Non Uniform stiffness

Level	El-Centro EQ			Mexico EQ			Chile EQ			New Zealand EQ		
	UD	25%	50%	UD	25%	50%	UD	25%	50%	UD	25%	50%
#	in/s^2	in/s^2	in/s^2	in/s^2	in/s^2	in/s^2	in/s^2	in/s^2	in/s^2	in/s^2	in/s^2	in/s^2
6	252	260	274	59.8	73.8	57.8	361	382	389	347	344	353
5	237	239	241	52.5	69.6	51	388	347	355	342	342	325
4	206	209	224	41.7	61.5	49.1	501	363	398	319	351	337
3	197	189	177	32.5	50.4	36	345	336	322	372	358	357
2	201	195	178	25.1	40	30.1	690	465	547	401	374	386
1	145	157	165	12.1	32.7	18.4	421	425	429	383	385	390
0	0	0	0	0	0	0	0	0	0	0	0	0

Table B.10 Six-story building variance calculation $(a-a_{avg})^2$ – Non Uniform stiffness

Level	El-Centro EQ			Mexico EQ			Chile EQ			New Zealand EQ		
#	UD	25%	50%	UD	25%	50%	UD	25%	50%	UD	25%	50%
6	2085.4	2686.7	4117.4	507.0	366.1	302.8	8100.0	18.8	312.1	186.8	225.0	25.0
5	940.4	950.7	971.4	231.5	223.0	112.4	3969.0	1547.1	2669.4	348.4	289.0	1089.0
4	0.1	0.7	200.7	19.5	46.7	75.7	2500.0	544.4	75.1	1736.1	64.0	441.0
3	87.1	367.4	1078.0	22.9	18.2	19.4	11236	2533.4	7168.4	128.4	1.0	1.0
2	28.4	173.4	1013.4	148.4	215.1	106.1	57121	6188.4	19693	1626.8	225.0	784.0
1	3761.8	2618.0	2010.0	634.2	482.5	484.0	900.0	1495.1	498.8	498.8	676.0	1024.0
0	0.0	0.0	0.0	0.0	0.0	0.0	0.0	0.0	0.0	0.0	0.0	0.0
Var	1380.7	1359.4	1878.2	312.7	270.3	220.1	16765	2465.5	6083.5	905.1	296.0	672.8

Table B.11 Eight-story building PFA – Non Uniform Stiffness

Level	El-Centro EQ			Mexico EQ			Chile EQ			New Zealand EQ		
	UD	25%	50%	UD	25%	50%	UD	25%	50%	UD	25%	50%
#	in/s^2	in/s^2	in/s^2	in/s^2	in/s^2	in/s^2	in/s^2	in/s^2	in/s^2	in/s^2	in/s^2	in/s^2
8	301	294	288	66.7	74	61.8	439	433	447	360	364	355
7	275	269	257	62.6	70	58.7	321	354	332	365	379	383
6	203	194	189	55.5	64.2	54.8	400	291	354	341	349	344
5	219	218	212	54.6	56.9	52.8	450	355	410	324	334	328
4	220	220	216	52.2	47	46.9	400	427	425	353	325	332
3	254	256	255	44.9	46.8	45.6	433	336	348	397	346	372
2	223	230	240	31.4	37.9	35	558	444	495	383	384	392
1	131	141	156	14.1	24.1	19.4	378	367	353	399	390	384
0	0	0	0	0	0	0	0	0	0	0	0	0

Table B.12 Eight-story building variance calculation $(a-a_{avg})^2$ – Non Uniform stiffness

Lev-el	El-Centro EQ			Mexico EQ			Chile EQ			New Zealand EQ		
#	UD	25%	50%	UD	25%	50%	UD	25%	50%	UD	25%	50%
8	5292.6	4389.1	3766.9	359.1	457.4	222.8	276.4	3263.3	2652.3	27.6	26.3	39.1
7	2185.6	1701.6	922.6	220.5	302.3	139.8	10276.9	478.5	4032.3	0.1	405.0	473.1
6	637.6	1139.1	1415.6	60.1	134.3	62.8	500.6	7204	1722.3	588.1	97.5	297.6
5	85.6	95.1	213.9	46.9	18.4	35.1	763.1	435.8	210.3	1701.6	618.8	1105.6
4	68.1	60.1	112.9	19.8	31.5	0.0	500.6	2614	870.3	150.1	1148	855.6
3	663.1	798.1	805.1	8.1	33.8	1.6	112.9	1590	2256.3	1008.1	165.8	115.6
2	27.6	5.1	178.9	267.3	216.5	141.0	18394	4641	9900.3	315.1	631.3	945.6
1	9457.6	7525.6	4987.9	1132.3	813.0	754.9	1969.1	78.8	1806.3	1139.1	968.8	517.6
0	0.0	0.0	0.0	0.0	0.0	0.0	0.0	0.0	0.0	0.0	0.0	0.0
Var	2631.1	2244.8	1772.0	302.0	286.7	194.0	4684.8	2901	3350.0	704.2	580.1	621.4

Appendix C

STAAD PRO. SAMPLE MODELS SCRIPTS

C.1 Stick Model for Four Story Building with El Centro EQ Record

```
STAAD SPACE
START JOB INFORMATION
ENGINEER DATE 02-Jul-18
END JOB INFORMATION
INPUT WIDTH 79
SET SHEAR
UNIT INCHES KIP
JOINT COORDINATES
1 0 0 0; 2 0 120 0; 3 0 240 0; 4 0 360 0; 5 0 480 0;
MEMBER INCIDENCES
1 1 2; 2 2 3; 3 3 4; 4 4 5;
DEFINE MATERIAL START
ISOTROPIC CONCRETE
E 3150
POISSON 0.17
DENSITY 8.7e-005
ALPHA 5e-006
DAMP 0.05
TYPE CONCRETE
G 1346.15
TYPE CONCRETE
```

```
STRENGTH FCU 4
STRENGTH FCU 4
END DEFINE MATERIAL
MEMBER PROPERTY AMERICAN
1 PRIS YD 33.808 ZD 33.808
MEMBER PROPERTY AMERICAN
2 PRIS YD 33.755 ZD 33.755
3 PRIS YD 33.81 ZD 33.81
4 PRIS YD 33.77 ZD 33.77
CONSTANTS
MATERIAL CONCRETE ALL
SUPPORTS
1 FIXED
2 FIXED BUT FX FY FZ MX MY KMZ 413000
3 FIXED BUT FX FY FZ MX MY KMZ 419400
4 FIXED BUT FX FY FZ MX MY KMZ 421500
5 FIXED BUT FX FY FZ MX MY KMZ 413000
DEFINE TIME HISTORY DT 0.01
TYPE 1 ACCELERATION SAVE
READ El-Centro.txt
ARRIVAL TIME
1
DAMPING 0.05
LOAD 2 LOADTYPE None  TITLE DYNAMIC
```

JOINT LOAD

2 FX 1078

3 FX 1078

4 FX 1078

5 FX 1078

MODAL CALCULATION REQUESTED

GROUND MOTION X 1 1 1.000000

PERFORM ANALYSIS

FINISH

C.2 Full 3D Model for Four Story Building

```
STAAD SPACE
START JOB INFORMATION
ENGINEER DATE 02-Jul-18
END JOB INFORMATION
INPUT WIDTH 79
SET SHEAR
UNIT INCHES KIP
JOINT COORDINATES
1 0 0 0; 2 0 120 0; 3 240 120 0; 4 480 120 0; 5 720 120 0; 6 960 120 0;
7 960 0 0; 8 720 0 0; 9 480 0 0; 10 240 0 0; 11 0 0 240; 12 0 120 240;
. . .
*Joint data was not included for space
6349 792 480 720; 6350 816 480 720; 6351 840 480 720; 6352 864 480 720;
6353 888 480 720; 6354 912 480 720; 6355 936 480 720;
MEMBER INCIDENCES
1 1 2; 2 2 1292; 3 3 1409; 4 4 1517; 5 5 1625; 6 6 7; 8 5 8; 10 4 9; 12 3 10;
13 11 12; 14 12 1400; 15 13 1508; 16 14 1616; 17 15 1724; 18 16 17; 19 15 18;
. . .
*Members incidences data was not included for space …
7322 6350 6351; 7323 6351 6352; 7324 6352 6353; 7325 6353 6354; 7326 6354
6355;
7327 6355 5104; 7329 2562 2547;
ELEMENT INCIDENCES SHELL
```

```
1538 2 1292 1293 1294; 1539 1292 1295 1296 1293; 1540 1295 1297 1298 1296;
1541 1297 1299 1300 1298; 1542 1299 1301 1302 1300; 1543 1301 1303 1304 1302;
. . .
*Shell members incidences data was not included for space …
6332 6340 6341 6351 6350; 6333 6341 6342 6352 6351; 6334 6342 6343 6353 6352;
6335 6343 6344 6354 6353; 6336 6344 6345 6355 6354; 6337 6345 6346 5104 6355;
ELEMENT PROPERTY
1538 TO 6337 THICKNESS 10
DEFINE MATERIAL START
ISOTROPIC CONCRETE
E 3150
POISSON 0.17
DENSITY 8.7e-005
ALPHA 5e-006
DAMP 0.05
TYPE CONCRETE
STRENGTH FCU 4
END DEFINE MATERIAL
MEMBER PROPERTY AMERICAN
1 6 8 10 12 13 18 TO 22 27 TO 31 36 TO 39 6338 6343 TO 6347 6352 TO 6356 6361
-
6362 TO 6365 6370 TO 6373 6668 6673 TO 6677 6682 TO 6686 6691 TO 6695 6700
-
6701 TO 6703 6998 7003 TO 7007 7012 TO 7016 7021 TO 7025 7030 TO 7032 -
7033 PRIS YD 16 ZD 16
2 TO 5 14 TO 17 23 TO 26 32 TO 35 43 TO 57 1259 TO 1537 6339 TO 6342 6348 -
6349 TO 6351 6357 TO 6360 6366 TO 6369 6374 TO 6667 6669 TO 6672 6678 TO
6681 -
6687 TO 6690 6696 TO 6699 6704 TO 6997 6999 TO 7002 7008 TO 7011 -
7017 TO 7020 7026 TO 7029 7034 TO 7327 7329 PRIS YD 16 ZD 12
CONSTANTS
MATERIAL CONCRETE ALL
SUPPORTS
1 7 TO 11 17 TO 21 27 TO 31 37 TO 40 FIXED
SLAVE FX FZ MASTER 1890 JOINT 2 TO 6 12 TO 16 22 TO 26 32 TO 36 1292
TO 2542
SLAVE FX FZ MASTER 3161 JOINT 2543 TO 3813
SLAVE FX FZ MASTER 4432 JOINT 3814 TO 5084
SLAVE FX FZ MASTER 5703 JOINT 5085 TO 6355
DEFINE TIME HISTORY DT 0.01
ARRIVAL TIME
1
DAMPING 0.05
```

```
UNIT FEET POUND
LOAD 3 LOADTYPE None  TITLE DYNAMIC ANALYSIS
SELFWEIGHT X 1
MEMBER LOAD
2 TO 5 32 TO 35 43 TO 45 55 TO 57 1259 TO 1268 1270 1272 1274 1276 1278 1280
-
1282 1284 1295 TO 1303 1322 TO 1330 1349 TO 1366 1376 1378 1380 1382 1384 -
1386 1388 1390 1392 1439 TO 1447 1457 1459 1461 1463 1465 1467 1469 1471 -
1473 1475 TO 1483 1493 TO 1501 1511 TO 1537 6339 TO 6342 6366 TO 6369 6374
-
6375 TO 6376 6386 TO 6398 6400 6402 6404 6406 6408 6410 6412 6414 -
6425 TO 6433 6452 TO 6460 6479 TO 6496 6506 6508 6510 6512 6514 6516 6518 -
6520 6522 6569 TO 6577 6587 6589 6591 6593 6595 6597 6599 6601 6603 6605 -
6606 TO 6613 6623 TO 6631 6641 TO 6667 6669 TO 6672 6696 TO 6699 6704 TO
6706 -
6716 TO 6728 6730 6732 6734 6736 6738 6740 6742 6744 6755 TO 6763 -
6782 TO 6790 6809 TO 6826 6836 6838 6840 6842 6844 6846 6848 6850 6852 6899
-
6900 TO 6907 6917 6919 6921 6923 6925 6927 6929 6931 6933 6935 TO 6943 6953
-
6954 TO 6961 6971 TO 6997 6999 TO 7002 7026 TO 7029 7034 TO 7036 7046 TO
7058 -
7060 7062 7064 7066 7068 7070 7072 7074 7085 TO 7093 7112 TO 7120 -
7139 TO 7156 7166 7168 7170 7172 7174 7176 7178 7180 7182 7229 TO 7237 7247
-
7249 7251 7253 7255 7257 7259 7261 7263 7265 TO 7273 7283 TO 7291 -
7301 TO 7327 7329 UNI GX 290
14 TO 17 23 TO 26 46 TO 54 1269 1271 1273 1275 1277 1279 1281 1283 -
1285 TO 1294 1304 TO 1321 1331 TO 1348 1367 TO 1375 1377 1379 1381 1383
1385 -
1387 1389 1391 1393 TO 1438 1448 TO 1456 1458 1460 1462 1464 1466 1468 1470
-
1472 1474 1484 TO 1492 1502 TO 1510 6348 TO 6351 6357 TO 6360 6377 TO 6385
-
6399 6401 6403 6405 6407 6409 6411 6413 6415 TO 6424 6434 TO 6451 -
6461 TO 6478 6497 TO 6505 6507 6509 6511 6513 6515 6517 6519 6521 -
6523 TO 6568 6578 TO 6586 6588 6590 6592 6594 6596 6598 6600 6602 6604 6614
-
6615 TO 6622 6632 TO 6640 6678 TO 6681 6687 TO 6690 6707 TO 6715 6729 6731
-
6733 6735 6737 6739 6741 6743 6745 TO 6754 6764 TO 6781 6791 TO 6808 6827 -
6828 TO 6835 6837 6839 6841 6843 6845 6847 6849 6851 6853 TO 6898 -
```

```
6908 TO 6916 6918 6920 6922 6924 6926 6928 6930 6932 6934 6944 TO 6952 6962
-
6963 TO 6970 7008 TO 7011 7017 TO 7020 7037 TO 7045 7059 7061 7063 7065
7067 -
7069 7071 7073 7075 TO 7084 7094 TO 7111 7121 TO 7138 7157 TO 7165 7167
7169 -
7171 7173 7175 7177 7179 7181 7183 TO 7228 7238 TO 7246 7248 7250 7252 7254
-
7256 7258 7260 7262 7264 7274 TO 7282 7292 TO 7300 UNI GX 270
ELEMENT LOAD
1538 TO 6337 PR GX 26.4
MODAL CALCULATION REQUESTED
UNIT INCHES KIP
LOAD 1 LOADTYPE Dead  TITLE DEAD
SELFWEIGHT Y -1
UNIT FEET POUND
MEMBER LOAD
2 TO 5 32 TO 35 43 TO 45 55 TO 57 1259 TO 1268 1270 1272 1274 1276 1278 1280
-
1282 1284 1295 TO 1303 1322 TO 1330 1349 TO 1366 1376 1378 1380 1382 1384 -
1386 1388 1390 1392 1439 TO 1447 1457 1459 1461 1463 1465 1467 1469 1471 -
1473 1475 TO 1483 1493 TO 1501 1511 TO 1537 6339 TO 6342 6366 TO 6369 6374
-
6375 TO 6376 6386 TO 6398 6400 6402 6404 6406 6408 6410 6412 6414 -
6425 TO 6433 6452 TO 6460 6479 TO 6496 6506 6508 6510 6512 6514 6516 6518 -
6520 6522 6569 TO 6577 6587 6589 6591 6593 6595 6597 6599 6601 6603 6605 -
6606 TO 6613 6623 TO 6631 6641 TO 6667 6669 TO 6672 6696 TO 6699 6704 TO
6706 -
6716 TO 6728 6730 6732 6734 6736 6738 6740 6742 6744 6755 TO 6763 -
6782 TO 6790 6809 TO 6826 6836 6838 6840 6842 6844 6846 6848 6850 6852 6899
-
6900 TO 6907 6917 6919 6921 6923 6925 6927 6929 6931 6933 6935 TO 6943 6953
-
6954 TO 6961 6971 TO 6997 6999 TO 7002 7026 TO 7029 7034 TO 7036 7046 TO
7058 -
7060 7062 7064 7066 7068 7070 7072 7074 7085 TO 7093 7112 TO 7120 -
7139 TO 7156 7166 7168 7170 7172 7174 7176 7178 7180 7182 7229 TO 7237 7247
-
7249 7251 7253 7255 7257 7259 7261 7263 7265 TO 7273 7283 TO 7291 -
7301 TO 7327 7329 UNI GY -290
14 TO 17 23 TO 26 46 TO 54 1269 1271 1273 1275 1277 1279 1281 1283 -
1285 TO 1294 1304 TO 1321 1331 TO 1348 1367 TO 1375 1377 1379 1381 1383
1385 -
```

```
1387 1389 1391 1393 TO 1438 1448 TO 1456 1458 1460 1462 1464 1466 1468 1470
-
1472 1474 1484 TO 1492 1502 TO 1510 6348 TO 6351 6357 TO 6360 6377 TO 6385
-
6399 6401 6403 6405 6407 6409 6411 6413 6415 TO 6424 6434 TO 6451 -
6461 TO 6478 6497 TO 6505 6507 6509 6511 6513 6515 6517 6519 6521 -
6523 TO 6568 6578 TO 6586 6588 6590 6592 6594 6596 6598 6600 6602 6604 6614
-
6615 TO 6622 6632 TO 6640 6678 TO 6681 6687 TO 6690 6707 TO 6715 6729 6731
-
6733 6735 6737 6739 6741 6743 6745 TO 6754 6764 TO 6781 6791 TO 6808 6827 -
6828 TO 6835 6837 6839 6841 6843 6845 6847 6849 6851 6853 TO 6898 -
6908 TO 6916 6918 6920 6922 6924 6926 6928 6930 6932 6934 6944 TO 6952 6962
-
6963 TO 6970 7008 TO 7011 7017 TO 7020 7037 TO 7045 7059 7061 7063 7065
7067 -
7069 7071 7073 7075 TO 7084 7094 TO 7111 7121 TO 7138 7157 TO 7165 7167
7169 -
7171 7173 7175 7177 7179 7181 7183 TO 7228 7238 TO 7246 7248 7250 7252 7254
-
7256 7258 7260 7262 7264 7274 TO 7282 7292 TO 7300 UNI GY -270
ELEMENT LOAD
1538 TO 6337 PR GY -26.4
LOAD 2 LOADTYPE Live  TITLE LIVE
ELEMENT LOAD
1538 TO 6337 PR GY -40
UNIT FEET KIP
PERFORM ANALYSIS
FINISH
```